generally used in order to assess the maximum current density which can be drawn from the cell without causing excessive overvoltages.

On an atomic level, in cells operating via an insertion mechanism, the maximum current density is limited by the chemical diffusion rate ($\tilde{D}$) of the mobile species. A number of studies has appeared over the past decade on theoretical and practical aspects of ion diffusion in solid state electrodes [116,117,119-123]. The basic principle in all these studies is that, in insertion electrodes, ion diffusion rates are determined by two factors: a kinetic component and a thermodynamic component.

The kinetic component is derived from Fick's Second Law of Diffusion, which relates the diffusion coefficient, D, to the concentration gradient as a function of time:

$$\frac{\partial c}{\partial t} = D \frac{\partial^2 c}{\partial x^2} \qquad (2.37)$$

with c = concentration
x = distance
t = time

In an ideal electrode, the surface concentration of the intercalate is related to the overvoltage, $\eta(t)$, by the Nernst equation:

$$\eta(t) = E_t - E_o = \frac{RT}{nF} \ln \frac{c_o}{c_t} \qquad (2.38)$$

where $\eta(t)$ = overvoltage at a time t
$E_{t,o}$ = cell potential at a time t and at equilibrium, respectively
R,T,n,F = as above
c = concentration of the intercalate

However, intercalation electrodes are seldom ideal; it is therefore necessary to introduce a thermodynamic component K_t:

$$K_t = \frac{\partial \ln a}{\partial \ln c} \qquad (2.39)$$

where a = activity of the intercalated ion
c = concentration of the intercalated ion

K_t is frequently referred to as the "thermodynamic" or "enhancement", or "Darken" factor [120,122].

2.6.2 The galvanostatic pulse-relaxation technique by Basu and Worrell

Several methods for the determination of chemical diffusion rates have been described in the literature [116,119,123]. Amongst the most frequently used methods is the galvanostatic pulse-relaxation technique by Basu and Worrell [116].

This method consists in inserting a small quantity of lithium ions into the host material, using a small current pulse: this causes the cell voltage to change from its equilibrium value. If a negligible quantity of Li^+ ions is inserted into the electrode, the overall stoichiometry remains essentially unchanged, and, after a time, the cell potential returns to its initial value. The evolution of the transient voltage with time reflects the Li^+ diffusion rate in the host structure.

A full mathematical treatment of this phenomenon goes beyond the scope of this work; however, a few salient equations will be recalled here.

However, intercalation electrodes are seldom ideal; it is therefore necessary to introduce a thermodynamic component K_t:

$$K_t = \frac{\partial \ln a}{\partial \ln c} \qquad (2.39)$$

where a = activity of the intercalated ion
c = concentration of the intercalated ion

K_t is frequently referred to as the "thermodynamic" or "enhancement", or "Darken" factor [120,122].

2.6.2 The galvanostatic pulse-relaxation technique by Basu and Worrell

Several methods for the determination of chemical diffusion rates have been described in the literature [116,119,123]. Amongst the most frequently used methods is the galvanostatic pulse-relaxation technique by Basu and Worrell [116].

This method consists in inserting a small quantity of lithium ions into the host material, using a small current pulse: this causes the cell voltage to change from its equilibrium value. If a negligible quantity of Li^+ ions is inserted into the electrode, the overall stoichiometry remains essentially unchanged, and, after a time, the cell potential returns to its initial value. The evolution of the transient voltage with time reflects the Li^+ diffusion rate in the host structure.

A full mathematical treatment of this phenomenon goes beyond the scope of this work; however, a few salient equations will be recalled here.

Fick's Second Law of Diffusion for semi-infinite geometry can be expressed as follows:

$$c - \bar{c} = \frac{i\tau}{FA(\pi\ Dt)^{1/2}} \exp\ (-a^2/4\ Dt) \qquad (2.40)$$

where i = current pulse [A]
τ = pulse duration [sec]
c = concentration of mobile ion [mol ml^{-1}]
$\bar{c}$ = initial concentration [mol ml^{-1}]
F = Faraday constant
A = electrode surface area
D = diffusivity [cm^2 sec^{-1}]
t = time [sec]
a = distance from planar source [cm]

Concentration can be expressed as follows:

$$c = \frac{x}{V} \qquad (2.41)$$

where x = composition in Li_x-(host)
V = molar volume [cm^3 mol^{-1}]

and can thus be linked to the cell voltages by the slope, m, of the electrochemical curve E = f(x). Equation (2.40) can thus be written as:

$$E - \bar{E} = \Delta E = \frac{m\ V\ i\ \tau}{FA\ (\pi\ Dt)^{1/2}} \quad (\text{with } a \simeq 0) \qquad (2.42)$$

The voltage difference ΔE is thus shown to be a linear function of $t^{-1/2}$. The slope, η, of $\Delta E = f\ (t^{-1/2})$ allows the calculation of the diffusion rate:

$$\tilde{D} = \frac{m\ V\ i\ \tau}{FA\ \pi^{1/2}\ \eta} \qquad (2.43)$$

Fick's Second Law of Diffusion for semi-infinite geometry can be expressed as follows:

$$c - \bar{c} = \frac{i\tau}{FA(\pi\ Dt)^{1/2}} \exp\ (-a^2/4\ Dt) \qquad (2.40)$$

where i = current pulse [A]
τ = pulse duration [sec]
c = concentration of mobile ion [mol ml^{-1}]
$\bar{c}$ = initial concentration [mol ml^{-1}]
F = Faraday constant
A = electrode surface area
D = diffusivity [cm^2 sec^{-1}]
t = time [sec]
a = distance from planar source [cm]

Concentrations can be expressed as follows:

$$c = \frac{x}{V} \qquad (2.41)$$

where x = composition in Li_x-(host)
V = molar volume [cm^3 mol^{-1}]

and can thus be linked to the cell voltages by the slope, m, of the electrochemical curve E = f(x). Equation (2.40) can thus be written as:

$$E - \bar{E} = \Delta E = \frac{m\ V\ i\ \tau}{FA\ (\pi\ Dt)^{1/2}} \quad (\text{with } a = 0) \qquad (2.42)$$

The voltage difference ΔE is thus shown to be a linear function of $t^{-1/2}$. The slope, η, of $\Delta E = f\ (t^{-1/2})$ allows the calculation of the diffusion rate:

$$\tilde{D} = \frac{m\ V\ i\ \tau}{FA\ \pi^{1/2}\ \eta} \qquad (2.43)$$

It is noted that variations of the kinetic component of the diffusion rate are reflected by n, whereas the thermodynamic component is included in the form of m.

2.6.3 Critical evaluation

The values of $\tilde{D}$ obtained by Basu and Worrell's method are subject to a few limitations, which are discussed here.

Firstly, diffusion rates obtained using polycrystalline samples only represent an average diffusion rate, and are insensitive to anisotropic effects, which are particularly pronounced in layered compounds. This setback can only be overcome with single crystals, as was shown by Spurdens and Steele for V_6O_{13} [124]. However, since practical batteries generally operate with polycrystalline electrodes, measurements on polycrystalline samples should be considered adequate.

A second drawback in Basu and Worrell's method, is the inaccuracy of the determination of the electrode surface area. This is generally approximated to be equal to the geometric area, which can be measured readily. It is generally accepted that the values obtained with this technique therefore only represent an upper limit for the diffusion rate [118], although recent results [125] show that this is not necessarily true.

Although the porosity of the electrode (and its consequent penetration by the electrolyte) is not taken into account, this factor is generally considered to be of decreasing importance as time increases during the experiment. For this reason, the slope n of $\Delta E = f\ (t^{-1/2})$ is measured when E approaches the equilibrium value.

Recently, Honders and Broers proposed a method for the determination of $\tilde{D}$ in polycrystalline samples, which has the advantage of combining the measurement of both the kinetic and the thermodynamic component in a single experiment [122,125]. Furthermore, this method is claimed to be more accurate, since the electrode surface area is not required, but only the electrode thickness is measured. This technique was not used in this work, due to the lack of suitable equipment.

The $\tilde{D}$ values determined here will be compared with data obtained by the same method within this work and elsewhere; for this purpose, they are considered acceptable. Finally, it must be noted that all existing methods for the determination of ion diffusion rates in solids are limited to single-phase systems; consequently $\tilde{D}$ will only be determined in the case of single-phase processes.

CHAPTER 3

GENERAL EXPERIMENTAL PROCEDURES

General experimental procedures used throughout this work, in particular lithium insertion and extraction by chemical means, the construction and operation of ambient temperature electrochemical cells, cyclic voltammetry cells, powder X-ray diffraction methods and differential scanning calorimetry experiments, are described in this chapter.

More specific details, e.g., quantities, starting materials and reaction times relating to the various systems studied in this work, are presented in separate sections in later chapters.

3.1 CHEMICAL LITHIATION WITH N-BUTYLLITHIUM

Chemical lithiation using n-butyllithium (n-BuLi) is known as a rapid and extremely effective method for inserting lithium into numerous compounds [28,33,77,126]. In particular the lithiation of an AB_2X_4 spinel can be expressed as:

$$2(AB_2)X_4 + 2C_4H_9\text{-}Li \longrightarrow 2Li^+(AB_2)^-X_4 + C_8H_{18}$$

Chemical lithiation was typically carried out under a nitrogen or argon atmosphere, using various amounts of n-BuLi (Merck, 15 w/o solution in hexane), which were injected into a stoppered flask containing 300 - 500 mg of the parent material in ~50 ml of sodium-dried hexane. The reaction mixture was stirred continuously at 50 °C for several days.

The products were washed several times with hexane in order to remove any excess n-BuLi, and finally dried under vacuum.

Stoichiometric quantities of n-BuLi were used when compounds with a specific composition were required. Excess n-BuLi was used to ensure that a fully lithiated product was obtained.

3.2 LITHIUM EXTRACTION BY CHEMICAL METHODS

In this work two methods were used to extract lithium from transition metal oxides containing lithium ($Li_xM_yO_z$).

3.2.1 Lithium extraction by bromine oxidation

Lithium can be extracted chemically using Br_2 according to the reaction:

$$LiM_yO_z + \frac{1-x}{2} Br_2 \longrightarrow Li_xM_yO_z + (1-x)LiBr$$

Stoichiometric or excess amounts of a 0.125 M $Br_2/CHCl_3$ solution were added to the lithium transition metal oxides, to obtain products with a desired composition.

The reaction flasks were kept in the dark, at ambient temperature with continuous stirring, generally for several days. Samples were filtered, washed several times with $CHCl_3$ and finally with EtOH to remove the lithium bromide by-product.

3.2.2 Lithium extraction by acid treatment

Lithium-containing compounds were treated with 1 N or 5 N H_2SO_4, to reduce the Li^+-ion content within their structures. Typically, 1 g of material was placed in ~15 ml of water, to which various amounts of acid were added. The reaction was allowed to continue for periods ranging from

one hour to several days, with constant stirring, at ambient temperature.

The solid products were filtered, washed several times with water and finally dried.

3.2.3 Lithium concentrations

Lithium concentrations of all samples that were litniated/ delithiated by chemical methods were determined by atomic absorption spectroscopy.

3.3 ELECTROCHEMICAL STUDIES

3.3.1 Electrochemical- and discharge-curve cells

A two-electrode cell was used in all ambient temperature electrochemical experiments for the determination of electrochemical and galvanostatic discharge curves and lithium diffusion rates.

The cell comprises a teflon casing and stainless-steel current collectors covered with teflon tape. Finely woven zirconia fabric soaked with the electrolyte was used to separate the electrodes.

A schematic representation of the cell is given in Fig 3.1.

Two electrolytes were used : $LiClO_4$ (Merck, G.R.) or $LiBF_4$ (Aldrich, 98 % pure), both 1M in distilled propylene carbonate (Merck or Fluka, 99% pure).

The lithium tetrafluoroborate was used as supplied. The lithium perchlorate was recrystallised in water and subsequently dried, first overnight in a drying oven at 80 °C, then under vacuum at 232 °C for several hours. The propylene carbonate was dried with 4 Å molecular sieves, and then distilled under vacuum (vapour phase temperature: 107-108 °C).

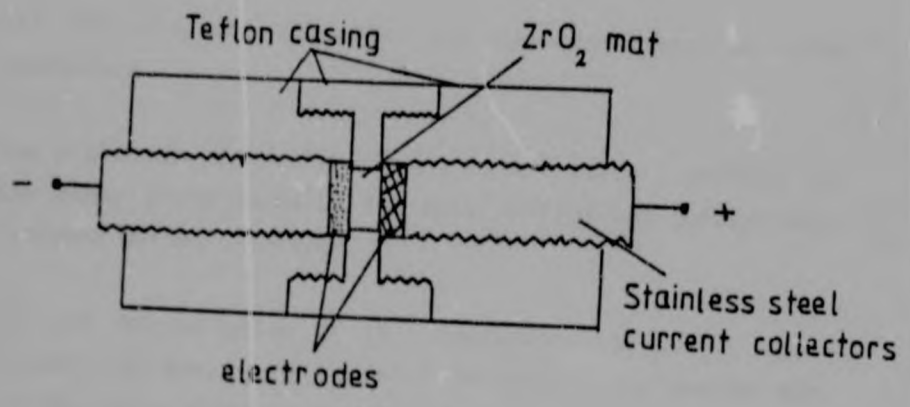

FIG 3.1
The ambient temperature electrochemical cell

The electrolytes were prepared and stored in a glove-box under an argon atmosphere. A 1 M concentration of the lithium salt was chosen in conformity with common practice and because this concentration yields the highest conductance in propylene carbonate [127].

Typical working electrodes consisted of 10-40 mg of powder compacted onto a 1 cm diameter stainless-steel gauze disc, at a pressure of 30-60 kN (9 - 18 MPa).

Counter-electrodes consisted either of a small piece of lithium metal or of ~100 mg of $LiMn_2O_4$ compacted onto a gauze disc, as in the case of the working electrodes. The spinel $LiMn_2O_4$ was used in preference to lithium metal during electrochemical lithium extraction experiments, in order to avoid high overpotentials and the formation of lithium dendrites. The spinel $LiMn_2O_4$ is known to incorporate lithium to form $Li_{1+x}Mn_2O_4$, a two-phase material over a wide range of x; it consists of a cubic and a tetragonal phase, and therefore operates as a constant voltage electrode [33]. It has been used successfully as a counter electrode to study the electrochemical extraction of lithium from $LiMn_2O_4$ [76].

All the cells were assembled and discharged under an argon atmosphere.

The cells were discharged at a constant current density, in the range 20-30 $\mu A/cm^2$. The cell voltage was continuously recorded during discharge.

For the determination of the electrochemical curve, open-circuit voltages were recorded intermittently during discharge, after allowing equilibration times of 48-72 hours.

The amount of lithium inserted into or extracted from the cathode (x), was obtained by coulombic titration; the theoretical electrode capacity, c [mA-hrs], assuming 1 Li reacts with each mole of the cathode, was calculated according to the expression:

$$c = I.t = \frac{m}{MW} \cdot \frac{N_A}{6.24 \cdot 10^{18}} \cdot \frac{1000}{3600} \qquad (3.1)$$

where c = theoretical electrode capacity [mA.hrs]
I = current
t = time
m = mass of cathode [g]
MW = molecular weight
N_A = Avogadro's constant
$6.24 \cdot 10^{18}$ = electronic charges per Coulomb
$\frac{1000}{3600}$ = conversion from A.s to mA.hrs
Note: $\frac{N_A}{6.24 \cdot 10^{18}} = F = 96485\ C\ mol^{-1}$

The theoretical energy density, calculated using the electrochemical curve, is given by the expression:

$$W_m = \frac{1}{m} \int_t EI \, dt = \frac{F}{MW \cdot 3600} \int_{\Delta x} E \, dx \qquad (3.2)$$

where W_m = energy density [Wh/kg]
MW = molecular weight [kg]
x = lithium inserted or extracted (cf text)
E = cell potential [V]
other symbols as defined previously.

3.3.2 Cyclic voltammetry cells

A three-electrode cell was used for cyclic voltammetry experiments. A diagram of the cell is presented in Fig. 3.2.

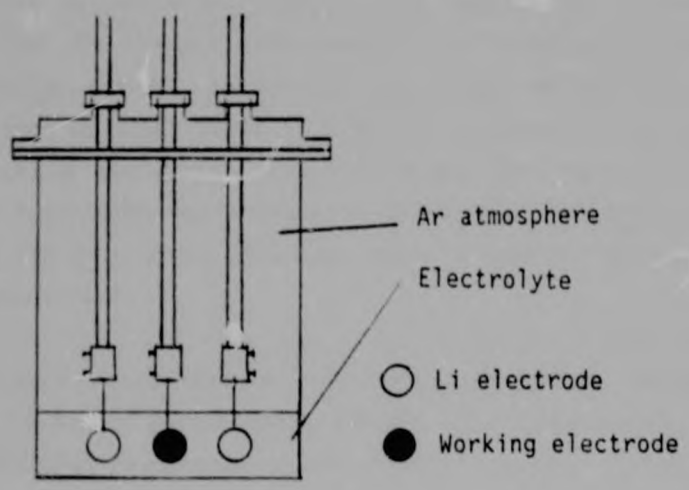

FIG. 3.2
The ambient temperature cyclic voltammetry cell

A piece of lithium, pressed onto an expanded nickel gauze disc was used as counter- and reference-electrode. The working electrode consisted of a few mg (1 - 4 mg) of transition metal oxide powder, pressed at 18 MPa onto an expanded nickel gauze disc.

The electrolyte used for cyclic voltammetry experiments was 1 M $LiClO_4$ in a 1:1 mixture of propylene carbonate (P.C.) and 1,2-dimethoxyethane (D.M.E.).

The purification of $LiClO_4$ and P.C. is given in section 3.3.1. The dimethoxyethane (Merck, >99% pure) was purified and dried by refluxing over sodium balls, followed by distillation under argon. The electrolyte was prepared and stored in a glove-box under an argon atmosphere.

The mixture of P.C. and D.M.E. solvents was favoured for cyclic voltammetry experiments, because it has a higher conductivity than pure P.C., probably due to complexation of the Li^+ ions by the ether [128]. This electrolyte is less suitable for the longer term experiments (electrochemical and discharge curves) because of the high volatility of D.M.E. Since no significant iR drop was observed across the electrolyte, a distance of 2.7 cm between the working and reference electrodes was considered acceptable. The cell was assembled and maintained under an argon atmosphere throughout the experiment.

The experiments were carried out using a Princeton Applied Research (P.A.R.) potentiostat (Model 173) linked to a P.A.R. Universal Programmer (Model 175).

Scan rates between 0.1 mV/sec and 1 mV/sec were used.

3.3.3 Determination of lithium diffusion rates

Lithium-ion diffusion rates were determined using the galvanostatic pulse-relaxation technique by Basu and Worrell [116], described in section 2.6.2.

Two-electrode cells, as described in section 3.3.1, were used. The current pulse was obtained from a P.A.R.

potentiostat Model 173 controlled by a P.A.R. Universal Programmer (Model 175). The pulse intensity was periodically checked before and after the experiments, by measuring the ohmic drop through a resistor. The size of the pulse varied between 50 μA $< i <$ 400 μA with 2 sec $< \tau <$ 10 sec, with typical values of i = 100 μA and τ = 5 sec. The value of the slope, η, of $\Delta E = f(t^{-1/2})$ was found to be reproducible when different size pulses were used. The cell voltage was monitored with a Fluke 8842A multimeter.

The slopes of the electrochemical curves (m), required in eq. 2.43, were determined in this work, unless otherwise stated.

3.4 POWDER X-RAY DIFFRACTION WORK

Powder X-ray diffraction spectra of most samples were recorded on an automated Rigaku powder diffractometer using CuK_α radiation with a graphite-crystal monochromator. Interplanar spacings were determined against an internal silicon standard.

Lattice parameters were refined with an existing computer program (Appleman), using the least-squares method. Structure determinations were carried out with an intensity refinement program developed by Wiseman [129]. Occupancies are given in terms of the number of atoms in a particular site, per formula unit.

The reliability factor R, calculated after each refinement, is given by eq. 2.17.

3.5 DIFFERENTIAL SCANNING CALORIMETRY (DSC)

All the differential scanning calorimetry experiments were performed on a Du Pont 1090 thermal analyser, using a standard 600 °C DSC cell.

Samples were hermetically sealed under argon in aluminium containers.

CHAPTER 4

LITHIUM EXTRACTION FROM $LiVO_2$

4.1 INTRODUCTION

Both the transition metals titanium and vanadium exhibit several stable oxidation states, and some of their oxides and sulphides are currently amongst the most studied systems as potential cathode materials for lithium batteries, e.g., TiS_2, VS_2, V_2O_5 and V_6O_{13} [13,21,22,85-93,130-132].

Although the isomorphous spinels $LiTi_2O_4$ and LiV_2O_4 are known, they are difficult to prepare in a pure state by conventional high temperature synthesis. In the course of a study on lithium insertion into anatase (TiO_2), Murphy and co-workers [77] obtained the pure spinel $LiTi_2O_4$ by heating anatase-related $Li_{0.5}TiO_2$ to temperatures above 500 °C.

In this work, a similar method for the preparation of LiV_2O_4 is proposed, using $Li_{0.5}VO_2$ as a starting material. The solid solution $Li_{1-x}VO_2$ ($0<x\leq1$) was recently obtained by Vidyasagar and Gopalakrishnan [133] by chemical oxidation of $LiVO_2$ with bromine. With this method, it is possible to prepare a compound with the stoichiometry $Li_{0.5}VO_2$, equivalent to that of the spinel LiV_2O_4. The conversion of $Li_{0.5}VO_2$ to the spinel LiV_2O_4 and the structural analysis of the latter is given in chapter 5.

In their paper on lithium extraction from $LiVO_2$, Vidyasagar and Gopalakrishnan briefly described the reaction and the products [133], but did not investigate fully the structural changes which take place during the extraction.

In order to understand the transformation of the compound $Li_{0.5}VO_2$ to the spinel structure LiV_2O_4, it was necessary to

investigate the structural characteristics of the former. The structural changes which occur during the reaction are indicative of the mobility of vanadium within the structure, a factor which is of relevance when considering the conversion to the spinel structure.

4.2 EXPERIMENTAL

$LiVO_2$ was prepared by reacting Li_2CO_3 (Koch-Light, 98% purity) and V_2O_5 (Merck, extra pure) in a 1:1 molar ratio, initially at 500 °C for 4 hours, to decompose the lithium carbonate, and then at 700 °C for 10 hours, under a hydrogen atmosphere [133].

$Li_{1-x}VO_2$ ($0<x<1$) was obtained using both chemical and electrochemical methods.

Chemical extraction of lithium from $LiVO_2$ was carried out by treating $LiVO_2$ with a 0.125 M solution of Br_2 in $CHCl_3$, according to the reaction:

$$LiVO_2 + \frac{(1-x)}{2} Br_2 \longrightarrow Li_xVO_2 + (1-x)LiBr \quad [133]$$

Stoichiometric quantities of bromine were used to prepare $Li_{0.5}VO_2$; smaller concentrations of lithium were obtained by using an excess of bromine solution. The mixtures were allowed to react for 4 days (unless otherwise specified).

A sample with the composition $Li_{0.44}VO_2$ was prepared by placing 300 mg $LiVO_2$ in 10 ml H_2O to which 7 ml of 1N H_2SO_4 were added. The reaction took place at ambient temperature, with constant stirring for 3 days. The blue colouring of the water indicated a partial dissolution of vanadium ions. The acidity of the solution was approximately pH = 1. The solid was filtered off, washed several times with H_2O and finally dried.

Lithium was extracted electrochemically from $LiVO_2$ in a two-electrode cell of the form:

$$LiVO_2 \,|\, 1M\ LiClO_4 \text{ in propylene carbonate} \,|\, LiMn_2O_4$$

The working- and the counter-electrode consisted of 20-30 mg of $LiVO_2$ and 120-150 mg of $LiMn_2O_4$ powders respectively, compacted onto stainless-steel gauze discs at a pressure of 50 kN.

Cells were discharged at a constant current density of $20\mu A/cm^2$. Equilibration times of up to 72 hours were allowed. The experiments were interrupted at different stages of the reaction in order to X-ray the resulting $Li_{1-x}VO_2$ ($0.3<x<0.95$) products.

4.3 RESULTS

The synthesis of the starting material $LiVO_2$ yielded a black powder which could be indexed to the trigonal space group $R\bar{3}m$, with a=2.840(1)Å and c=14.785(7)Å (Fig 4.1), consistent with the values reported in the literature (a=2.84Å and c=14.70Å) [134].

Atomic absorption analysis gave a lithium content of 7.71%, in excellent agreement with the theoretical value of 7.72% for the stoichiometry $Li_{1.0}VO_2$.

The powder X-ray diffraction patterns of various samples of $Li_{1-x}VO_2$ ($0<x<1$) indicated identical structural characteristics for the same values of x, whether the product had been prepared by chemical oxidation or electrochemically.

Initially, the extraction of lithium leaves the structure apparently unaltered : for the range $0<x<0.3$ the product was single-phase (phase I). The X-ray diffraction profiles were very similar to that of $LiVO_2$, with little change in the lattice parameters, "a" and "c", or in the relative intensities of the peaks. For

$0.3<x<0.7$, all the samples obtained both electrochemically and by chemical reaction had two-phase powder X-ray diffraction patterns: as in the case of phase I, phase II could be indexed to the trigonal space group $R\bar{3}m$ (Fig 4.2).

A sample with the composition $Li_{0.44}VO_2$, obtained by treating $LiVO_2$ with H_2SO_4, had the same two-phase pattern as the products obtained electrochemically and by bromine oxidation.

Further extraction of lithium ($0.7<x<0.9$) yields a single-phase compound (Fig 4.3). This product (phase II) has an increased lattice constant "a" and a smaller value of "c" compared to the parent compound $LiVO_2$; shifts in the interplanar spacings showed that the lattice constants approach cubic symmetry.

The lattice parameters of several samples of different composition, together with their method of preparation, are presented in Table 4.1. In the case of two-phase material, the lattice constants of both unit cells were refined only if the intensity and resolution of the peaks allowed it; this was not possible for $x=0.37$ and $x=0.70$, where only the peaks of the predominant phase were sharp enough to take an accurate measurement of 2θ.

TABLE 4.1

Lattice parameters and method of preparation of various samples of $Li_{1-x}VO_2$

x	Phase	a[Å]	c[Å]	Preparation
0	-	2.840(1)	14.785(7)	-
0.37	I(two-phase)	2.840(1)	14.799(4)	Electrochemical
0.50	I	2.841(1)	14.785(6)	Br_2 oxidation
	II	2.889(2)	14.241(13)	
0.70	II(two-phase)	2.886(1)	14.241(8)	Electrochemical
0.78	II	2.887(1)	14.230(8)	Br_2 oxidation
0.95*	II	2.886(1)	14.244(1)	Electrochemical

* Theoretical composition, calculated by coulombic titration.

Powder X-ray diffraction patterns of $LiVO_2$, $Li_{0.5}VO_2$ (characteristic of the two-phase range) and $Li_{0.22}VO_2$ are shown in Figs 4.1 - 3; the latter is described in Table 4.2.

The progress of the reaction was clearly visible from the X-ray diffraction patterns of electrodes with the composition $Li_{0.63}VO_2$, $Li_{0.50}VO_2$ and $Li_{0.30}VO_2$, where the relative intensities of the two phases gradually changed, showing an increasing quantity of phase II as the lithium concentration decreased. The product $Li_{0.22}VO_2$ was virtually single-phase, with a very minor trace of phase I; electrochemically prepared $Li_{0.05}VO_2$ was very similar, except for small quantities of unidentified decomposition products.

Chemical delithiation beyond the composition $Li_{0.22}VO_2$ could not be obtained even after treating $LiVO_2$ with excess bromine for 21 days. However, the samples contained small quantities of phase I, which could account for the relatively high lithium content compared to $Li_{\sim 0.1}VO_2$, reported by Vidyasagar and Gopalakrishnan [133].

As it can be observed in Fig 4.3, the relative intensities of the peaks of phase II differ considerably from those of $LiVO_2$; this is particularly noticeable in the case of the {003} peak, which decreases sharply in intensity.

The change of relative intensities is indicative of an atomic rearrangement of the relatively heavy vanadium ions within the oxide sublattice.

4.4 STRUCTURE OF $Li_{0.22}VO_2$

4.4.1 Structure determination

The structure of $Li_{0.22}VO_2$, corresponding to phase II was determined by an intensity refinement of the peaks of the

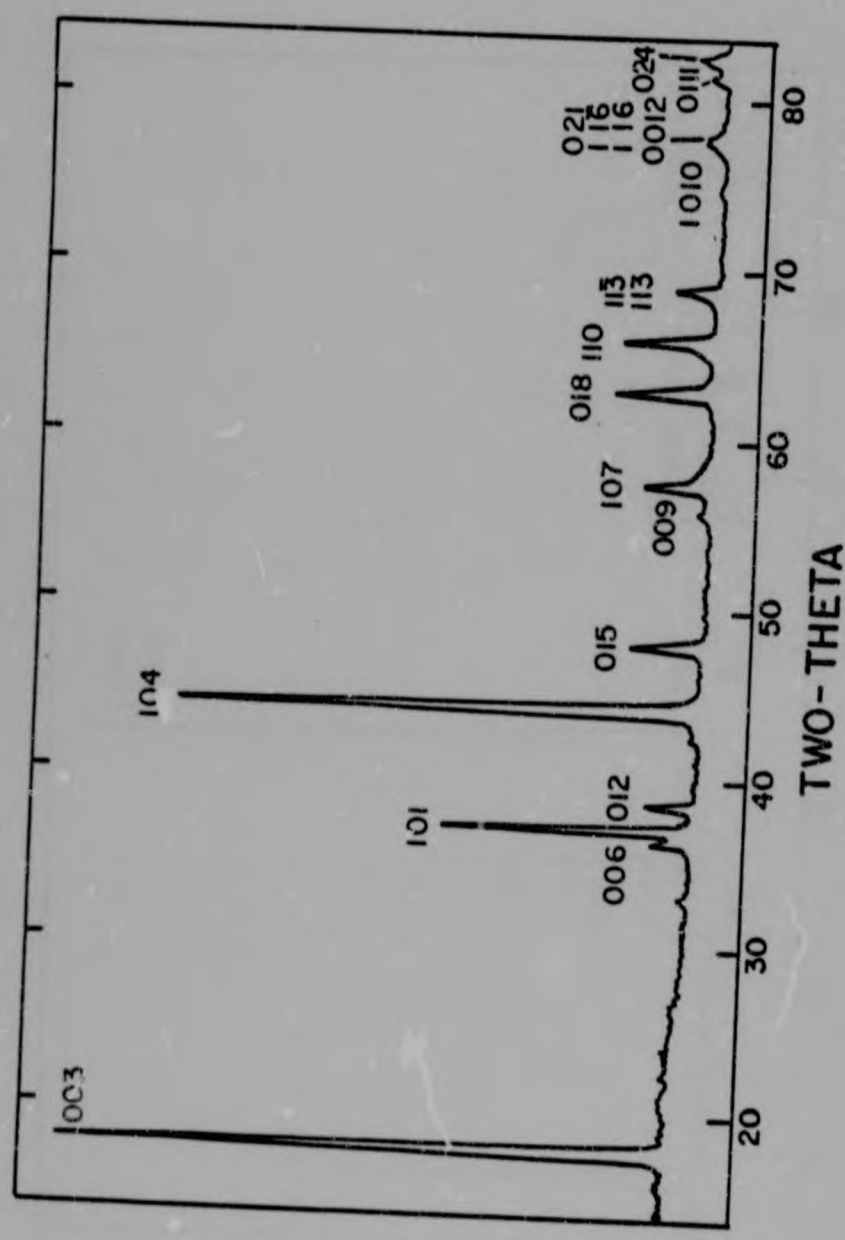

FIG 4.1
X-ray diffraction pattern of $LiVO_2$

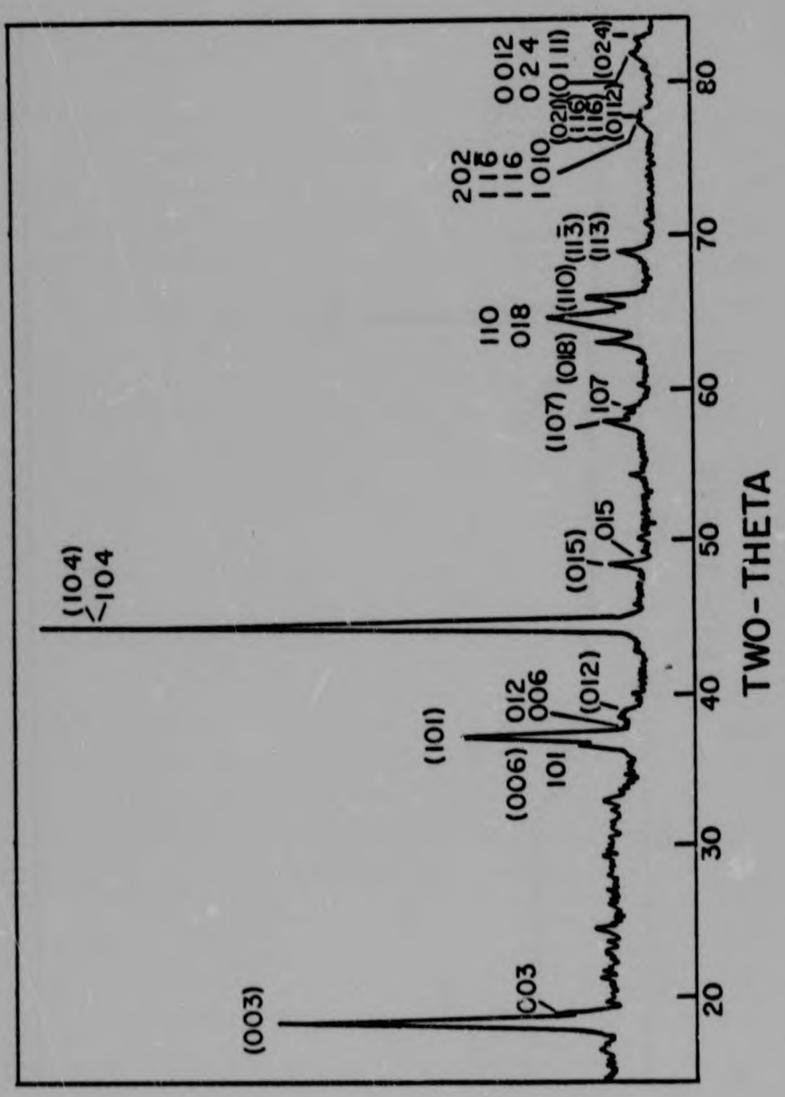

FIG 4.2

X-ray diffraction pattern of $Li_{0.5}VO_2$

Miller indices of Phase I are given in parentheses

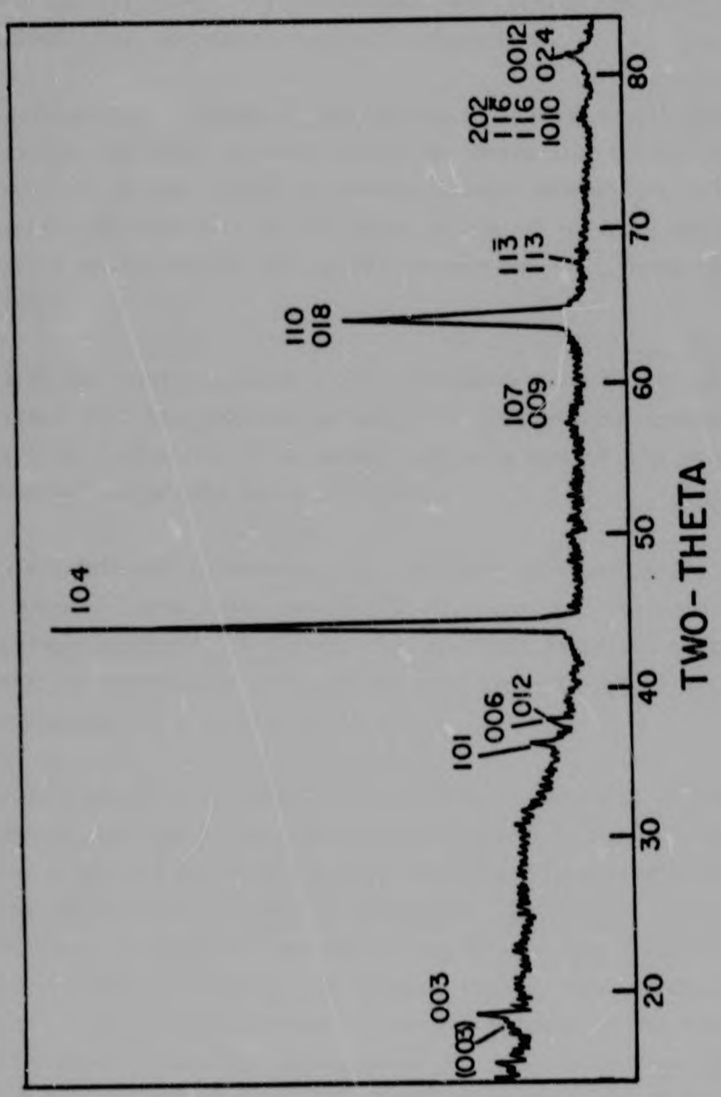

FIG 4.3
X-ray diffraction pattern of $Li_{0.2}VO_2$

X-ray diffraction pattern (Fig 4.3, Table 4.2). Because of overlapping peaks, the refinement was carried out with 12 intensities, corresponding to 23 reflections.

A preliminary attempt to refine the structure whilst maintaining the $LiVO_2$ layered structure, where the lithium and vanadium cations occupy alternate planes between the oxide layers, did not reflect the sharp change of relative intensities which occurs during the extraction of lithium from $LiVO_2$.

As it has been suggested in the preceding section, it seems likely that the observed variation of the relative intensities is indicative of an atomic rearrangement of the vanadium cations within the structure.

This hypothesis is based on the fact that vanadium (Z=23) is a heavier atom than lithium (Z=3), and is therefore a stronger scatterer of X-rays: any important variation of the relative intensities is therefore most probably due to a rearrangement of the vanadium ions.

In this section, it is postulated that the remaining lithium cations continue to reside in the octahedral 3a sites, which they occupy in the starting material $LiVO_2$. In a recent neutron diffraction study of $Li_{0.27}VO_2$ [135], the lithium cations were found to be distributed between the octahedral and tetrahedral sites of the lithium layer. This distribution of the lithium cations is ignored throughout the X-ray diffraction intensity refinements: it is assumed that the weak X-ray scattering power of small concentrations of lithium cations would not significantly affect the results of this study. In order to account for the modification of the relative intensities, a rearrangement of the structure was proposed, in which a fraction of the vanadium ions migrates to the layer which was initially occupied exclusively by lithium.

The vanadium cations in the lithium-deficient phase, which have a formal valence of $V^{4+/3+}$, were permitted to occupy the octahedral sites 3a and 3b; the site occupancy (n) in those sites was allowed to vary, whilst the total number of vanadium ions was constrained to unity (as is required by stoichiometry).

The isotropic temperature factors (B_{iso}) of the vanadium cations were varied independently of the site occupancy after the latter had been fixed. The positional coordinate (z) and the temperature factor of the oxide ions were also refined.

The lithium concentration was maintained constant at 0.2 (as obtained by atomic absorption spectroscopy) and the temperature factor was arbitrarily fixed at $1Å^2$.

This model gave a final R value of 13.0% for a structure in which approximately one-third of the vanadium ions occupy the 3a sites, formerly filled by lithium cations; the rest of the vanadium ions remain in the 3b sites, which they occupy in the parent compound $LiVO_2$.

It is interesting to note that the anion positional parameter, z, refines to 0.250(2), a value that corresponds to a cubic structure: as it has already been pointed out in the preceding section, the lattice constants of phase II approach those of a cubic cell.

The full structural parameters of this model (model 1) are described in Table 4.3a, the observed and calculated intensities in Table 4.3b.

The octahedral sites 3a and 3b are interconnected by two sets of face-sharing tetrahedra in 6c positions. If the vanadium ions migrate via the faces of the octahedra, and

TABLE 4.2

Powder X-ray diffraction pattern of $Li_{0.2}VO_2$

Space group : $R\bar{3}m$
a=b=2.887(1)Å c=14.230(8)Å α=β=90° γ=120°

hkl	d_{obs}*	d_{calc}[Å]	I_{obs}**
003	4.759	4.742	126
101	2.461	2.462	76
006	2.371	2.371	36
012	2.358	2.358	
104	2.045	2.045	1000
015	1.879	1.878	17
009	1.580	1.581	25
107	1.580	1.577	
018	1.450	1.449	526
110	1.444	1.443	
113	1.382	1.381	30
$11\bar{3}$	1.382	1.381	
1 0 10	-	1.236	
116	1.232	1.233	35
$1\bar{1}6$	1.232	1.233	
202	-	1.231	
0 0 12	-	1.185	84
024	1.179	1.179	
208	1.022	1.022	62
1 1 12	0.916	0.916	
1 1 $\overline{12}$	0.916	0.916	74
$12\bar{}$	-	0.913	
214	-	0.913	

* Where no d_{obs} is indicated, the peak was weak and diffuse.

** Normalised to 1 000

TABLE 4.3a

Structural parameters of $Li_{0.2}VO_2$ (Model 1)

Space group $R\bar{3}m$ (D_{3d}^5) a = 2.887(1)Å c = 14.230(8)Å

ATOM	POSITION	x	y	z	B[Å^2]	n
Li^+	3a	0	0	0	1.0	0.2
$V^{3+/4+}$	3a	0	0	0	1.8(13)	0.34(3)
$V^{3+/4+}$	3b	0	0	0.5	1.7(8)	0.66(3)
O^{2-}	6c	0	0	0.250(2)	3.2(9)	2.0

(Mean valence state of vanadium: 3.8)

TABLE 4.3b

Observed and calculated intensities for $Li_{0.2}VO_2$ (Model 1)

R = 13.0 %

hkl	I_{obs}	I_{calc}	hkl	I_{obs}	I_{calc}
003	98	116	113	23	12
101	59	58	$11\bar{3}$		
006	28	24	1 0 10		
012			116	27	27
104	774	797	$11\bar{6}$		
015	13	22	202		
009	19	15	0 0 12	65	73
107			024		
018	407	317	208	48	28
110			1 1 12		
			1 1 $\overline{12}$	57	79
			$12\bar{4}$		
			214		

not via the edges, they would have to transit through a tetrahedral site. This would seem a likely pathway, as it avoids the narrow bottleneck constituted by the two oxide ions situated at the ends of the O-O edge.

In model 2, the vanadium ions were allowed to occupy all the available octahedra and tetrahedra in the unit cell; the fractional coordinates of the tetrahedral sites were taken as (0, 0, 0.125) and (0, 0, 0.375) because of the almost cubic symmetry.

The refinement was carried out without imposing any restrictions on the total quantity of vanadium; a B_{iso} factor of $2Å^2$, close to that obtained in model 1, was chosen for all the vanadium ions, and was not refined.

As in model 1, the oxygen positional parameter and the B_{iso} factor were refined; the lithium ion occupancy and temperature factor were kept constant, with a value of 0.2 and $1Å^2$ respectively.

This refinement gave a final R value of 4.0 %, which is considerably lower than the one obtained for model 1. The vanadium occupancy refined to 0.10(3) and 0.06(3) in the tetrahedral sites of the original vanadium and lithium layers respectively, whereas the distribution of the vanadium ions in the octahedral sites 3a and 3b did not alter significar ly compared to model 1.

The sum of the vanadium ions obtained according to this model is 1.16(12), which, within experimental error, is close to the value required by the formula $Li_{0.2}VO_2$.

The structural parameters of model 2 are given in Table 4.4a, the observed and calculated intensities in Table 4.4b.

TABLE 4.4a

Structural parameters of $Li_{0.2}VO_2$ (Model 2)

Space group $R\bar{3}m$ (D_{3d}^5) a = 2.887(1)Å c = 14.230(8)Å

Atom	Position	x	y	z	B[Å^2]	n
Li^+	3a	0	0	0	1.0	0.2
$V^{3+/4+}$	3a	0	0	0	2.0	0.36(2)
$V^{3+/4+}$	3b	0	0	0.5	2.0	0.64(4)
V^{5+}	6c	0	0	0.125	2.0	0.06(3)
V^{5+}	6c	0	0	0.375	2.0	0.10(3)
O^{2-}	6c	0	0	0.249(1)	3.4(8)	2.0

TABLE 4.4b

Observed and calculated intensities for $Li_{0.2}VO_2$ (Model 2)

R = 4.0 %

hkl	I_{obs}	I_{calc}	hkl	I_{obs}	I_{calc}
003	98	103	1 0 10		
101	59	61	116	27	29
006	28	27	$11\bar{6}$		
012			202		
104	774	766	0 0 12	65	64
015	13	13	024		
009	19	17	208	48	35
107			1 1 12		
018	407	417	1 1 $\overline{12}$	57	65
110			$12\bar{4}$		
113	23	9	214		
$11\bar{3}$					

A further refinement of model 2, in which the B_{iso} factors of the vanadium ions in 3a and 3b, as well as the oxide positional parameter and the temperature factor were allowed to vary, did not significantly alter any of the variables : B_{iso} of the vanadium ions in 3a and 3b refined to 2.5(6)$Å^2$ and 1.8(4)$Å^2$ respectively; the other parameters remained constant. The R value was almost unchanged, with a value of 4.5 %.

Attempts to refine the B_{iso} factors of the vanadium ions in the tetrahedral sites failed, predominantly because of the strong correlation with the low occupancy of those sites, and also because of the relatively small number of intensities available for the refinement.

However, several independent refinements were carried out, in which the vanadium B_{iso} factors were fixed at various values; the same procedure was used as for model 2. Since most of the structures obtained were almost identical to model 2, only two of them (models 3 and 4) will be reported here.

In model 3, the B_{iso} factors were fixed at 2.0$Å^2$ and 1.0$Å^2$ for the vanadium ions in the octahedral and in the tetrahedral sites respectively.

The R value of 3.6 % for this model is slightly lower than for model 1, although the structural parameters (Table 4.5) only differ very slightly from model 2.

In spite of the slightly higher R value, model 2 is preferred over model 3, because the vanadium ions in the tetrahedral sites would be expected to be at least as mobile as those in the octahedral sites. This mobility should be reflected by the B_{iso} factors, which express the average thermal displacement of the atom in the lattice.

TABLE 4.5

Structural parameters of $Li_{0.2}VO_2$ (Model 3)

R = 3.6 %

Space group $R\bar{3}m$ (D^5_{3d}) a = 2.887(1)Å c = 14.230(8)Å

Atom	Position	x	y	z	B[Å^2]	n
Li^+	3a	0	0	0	1.0	0.2
$V^{3+/4+}$	3a	0	0	0	2.0	0.36(2)
$V^{3+/4+}$	3b	0	0	0.5	2.0	0.65(4)
V^{5+}	6c	0	0	0.125	1.0	0.05(2)
V^{5+}	6c	0	0	0.375	1.0	0.09(2)
O^{2-}	6c	0	0	0.249(1)	3.2(7)	2.0

Finally, in model 4, the isotropic temperature factors of all the relatively heavy vanadium ions were fixed at 1.0Å^2.

Although the R value (8.4 %) was higher than in models 2 and 3, the interest of model 4 lies in the fact that the sum of all the vanadium ions, 1.07(18), is closer to unity than in model 2, where it amounted to 1.16(12), while maintaining the presence of vanadium ions in the tetrahedral sites. The full atomic parameters of model 4 are listed in Table 4.6.

TABLE 4.6

Structural parameters of $Li_{0.2}VO_2$ (Model 4)

R = 8.4 %

Space group $R\bar{3}m$ (D^5_{3d}) a = 2.887(8)Å c = 14.230(1)Å

Atom	Position	x	y	z	B[Å^2]	n
Li^+	3a	0	0	0	1.0	0.2
$V^{3+/4+}$	3a	0	0	0	1.0	0.32(4)
$V^{3+/4+}$	3b	0	0	0.5	1.0	0.61(6)
V^{5+}	6c	0	0	0.125	1.0	0.05(4)
V^{5+}	6c	0	0	0.375	1.0	0.09(4)
O^{2-}	6c	0	0	0.248(2)	3.4(11)	2.0

4.4.2 Discussion

The structural characterisation of $Li_{0.22}VO_2$ may be summarised as follows: the layered structure of $LiVO_2$, in which lithium and vanadium ions occupy alternate layers of octahedral sites, is not maintained in $Li_{0.22}VO_2$.

In model 1, which gave an R value of 13.0%, approximately one-third of the vanadium ions were found to be located in the octahedral 3a sites, i.e., in the layer previously occupied solely by lithium, with the remaining two-thirds in their original vanadium layer, in the octahedral positions 3b.

Noting that the octahedral sites are interconnected by face-sharing tetrahedra, a refinement in which the vanadium ions occupied both the octahedral and the tetrahedral positions was carried out. This model (model 2) yielded a significantly lower R value (4.0%), and showed that a small, but not negligible proportion of vanadium ions is situated in the tetrahedral sites; the remainder are located in the octahedral sites of the two layers, with approximately the same distribution as was obtained in model 1.

Since V^{4+} seldom adopts a tetrahedral coordination in vanadium oxides [136], it is suggested that, upon migration, the V^{4+} cation is oxidised to V^{5+}, via the disproportionation reaction:

$$2V^{4+}_{oct,3b} \longrightarrow V^{3+}_{oct,3b} + V^{5+}_{tetr.} \qquad (4.1)$$

During the transfer of the pentavalent vanadium to an empty octahedral site in the lithium layer, an electron is recaptured:

$$V^{5+}_{tetr} + V^{3+}_{oct,3b} \longrightarrow V^{4+}_{oct,3a} + V^{4+}_{oct,3b} \qquad (4.2)$$

All these electron transfers are accessible, as the energy separation of the $V^{3+/4+}$ and $V^{4+/5+}$ couples is less than 2 eV [137].

The overall result of the transfer is finally:

$$V^{4+}_{oct,3b} + \square_{oct,3a} \longrightarrow \square_{oct,3b} + V^{4+}_{oct,3a} \quad (4.3)$$

This process could well be the mechanism by which the migration of vanadium ions occurs from the 3b to the 3a sites, particularly in view of the fact that model 2 indicates the presence of vanadium in the tetrahedral sites.

The transfer of the vanadium ions from the 3b sites to the depleted lithium layer has the effect of stabilising the structure: the vanadium ions replace the lithium ions, and maintain the necessary electrostatic bonding between the oxide layers.

The question of the partial occupancy of the tetrahedral sites by vanadium cations remains, to a certain extent, uncertain.

It may be remarked that it is unlikely that face-sharing octahedra and tetrahedra are simultaneously occupied by tetra- and pentavalent cations respectively, because of the strong electrostatic repulsion between ions of the same sign, which would be situated at 1.779Å from each other.

However, several considerations support the findings of model 2.

The simultaneous occupancy of octahedral and tetrahedral positions does not necessarily imply that the cations are situated in adjacent sites. As the process of delithiation advances, several 3a sites become vacant, increasing the

probability of obtaining three empty 3a octahedra which share faces with a particular tetrahedron in the lithium layer. The vanadium may then migrate from the 3b to the 3a sites, creating, in turn, several vacancies in the layer of 3b octahedra.

It is therefore conceivable that some of the tetrahedral sites in the vanadium layer will then be surrounded by three vacant octahedra, namely one 3a and two 3b sites, and by one occupied 3b site, containing a vanadium ion. The latter could then transfer to that tetrahedral site, as there would be no other cations in close proximity.

Although most of the vanadium ions in the tetrahedral sites continue their movement into the 3a sites, it cannot be excluded that a small percentage might remain in the 6c sites. This could be especially true during the last stages of the migration, when a number of ions sufficient to stabilise the structure has already reached the 3a sites.

It is worth noting that, according to models 2 - 4, the number of vanadium ions occupying the tetrahedra at (0,0,0.375), situated in the original lithium layer, is almost double that of the cations in the tetrahedra of the vanadium layer, at (0,0,0.125).

According to model 2, the 3a sites have a combined lithium and vanadium occupancy of 0.56, whereas the 3b sites are 64% full; a consequence of this is that tetrahedral sites sharing faces with three empty octahedra will be encountered more frequently in the lithium layer than in the vanadium layer. The occupancies obtained in models 2 - 4 are consistent with this observation, and seem to confirm that the vanadium ions are situated in tetrahedral sites only if the latter share faces with vacant octahedra.

If the tetrahedral sites are indeed partially occupied by pentavalent vanadium cations, then V^{3+}, V^{4+} and V^{5+} would coexist in $Li_{0.22}VO_2$. Although this cannot be proven by more common analytical techniques, because of the rapid equilibria that occur in solution, it must be stressed that the disproportionation reaction (eq. 4.1) is known to take place with relative ease [137].

A comparison between the V-O distances and the sum of the ionic radii appears to support this hypothesis : the combined ionic radii of the oxide ion and of V^{5+} in the tetrahedral coordination amount to 1.755Å [138], a value which compares favourably with the V-O distance of 1.779Å in the 6c tetrahedral sites.

Furthermore, the bond length in the 3a and 3b octahedra is 2.046Å; this value is close to the sum of the ionic radii of V^{3+} - O^{2-} and V^{4+} - O^{2-}, which amounts to 2.04Å and 1.98Å respectively [138].

Finally, coexistence of V^{3+}, V^{4+} and V^{5+} within the same structure is possible not only because of the small energy separation between the $V^{4+/5+}$ and the $V^{3+/4+}$ couples, but also because the ions occupy crystallographically different sites; it has previously been suggested in order to explain the electrical properties of the spinel $Li_{0.6}Zn_{0.8}V_{1.6}O_4$ [139].

All the points mentioned above seem to indicate that the structure proposed in model 2, where vanadium ions occupy the 6c tetrahedral sites, as well as the 3a and 3b octahedral sites, is not unreasonable.

However, the isotropic temperature factors of the vanadium ions refine to 1.8(13)Å^2 and 1.7(8)Å^2 in 3a and 3b respectively in model 1; similar values (2.5(6)Å^2 and 1.8(4)Å^2) were obtained upon further refinement (model 2). These B_{iso} factors are unusually high for the comparatively heavy transition metal ions, as is evident when they are

compared to other lithium intercalated transition metal oxides, where the B_{iso} factors of the transition metal cations are generally in the order of 0.5-1.0 A^2 [33,78].

The B_{iso} factors reflect the average displacement of an atom within the structure due to thermal vibrations. The abnormally high values obtained for the vanadium ions in $Li_{0.22}VO_2$ indicate that these ions are particularly mobile. It is therefore possible that the partial occupancy of the 6c tetrahedral sites is due to mobile vanadium ions that do not remain fixed in their more common octahedral coordination. The structure proposed in model 2 would then reflect an average representation of different, time-dependent situations.

4.5 ELECTROCHEMICAL CHARACTERISATION

4.5.1 Electrochemical curve

In the course of the electrochemical reaction, lithium is extracted from $LiVO_2$ and inserted into $LiMn_2O_4$. The electrochemical curve, which shows the open-circuit-voltage (o.c.v) against the composition of $Li_{1-x}VO_2$, expressed as a function of x, is given in Fig 4.4. It consists of three sections: for $0<x<0.3$ there is a continuous drop of the voltage, indicating the presence of a single-phase material, which was found to correspond to phase I (cf section 4.3).

In the range $0.3<x<0.85$ the curve flattens and the reaction appears to have an almost two-phase character. A slight slope is sometimes observed in the case of two-phase reactions, where a constant voltage plateau is expected.

This is often due to the relatively short equilibration times of 48 - 72 hours. Extremely long periods would be required for the system to reach absolute equilibrium (e.g.

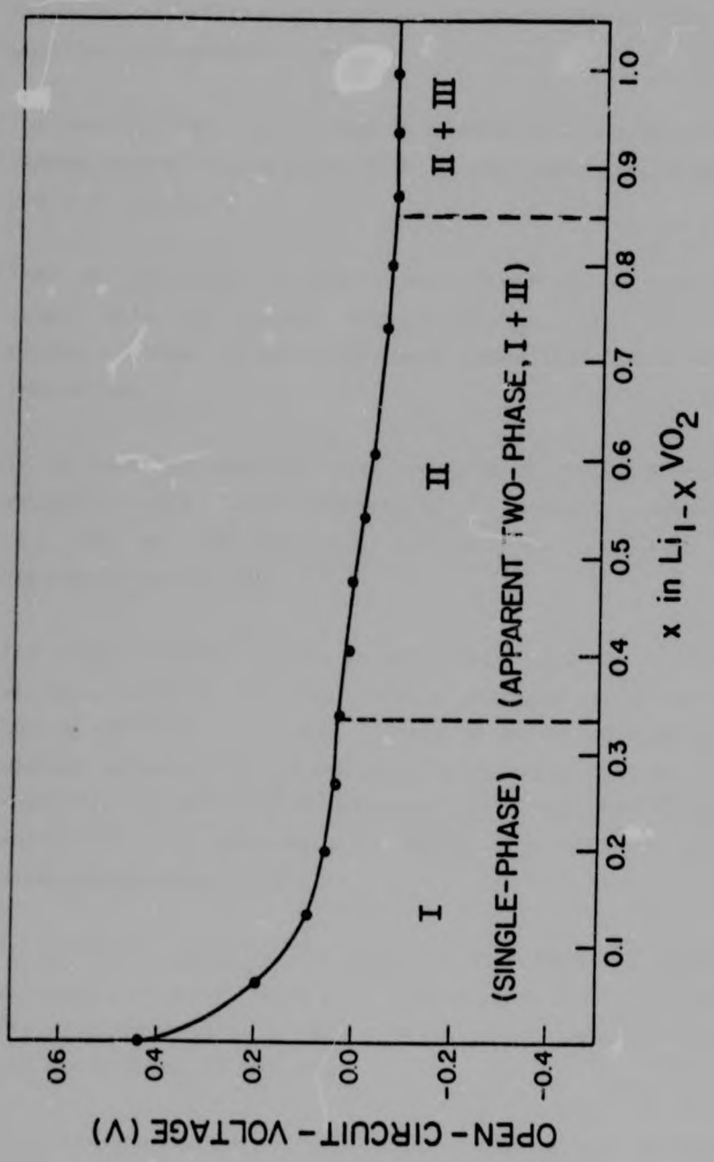

FIG 4.4

Ambient temperature electrochemical curve of the cell

$LiVO_2 \,|\, LiClO_4$ 1M(P.C.) $|\, LiMn_2O_4$

several weeks) , and to observe a two-phase voltage plateau. X-ray powder diffraction patterns of electrodes of this composition show phases I and II.

For $x \geq 0.85 \pm 0.05$, the voltage is constant; this plateau continues beyond the possible limit of x=1, indicating a decomposition reaction.

This was confirmed by the X-ray diffraction pattern of a sample with the nominal composition $Li_{0.05}VO_2$, which included a number of relatively weak peaks that could not be identified.

It is therefore doubtful that complete delithiation can be reached : the final composition is probably closer to $Li_{\sim 0.1}VO_2$ as was obtained chemically by Vidyasagar and Gopalakrishnan [133].

The electrochemical curve, in conjunction with the structural data, suggests that the reaction proceeds along the following pathway: initially lithium is extracted from $LiVO_2$ without altering the structure significantly. Phase I is therefore a delithiated compound $Li_{1-x}VO_2$, for $0<x\leq 0.3$, which cannot be distinguished easily from $LiVO_2$ by powder X-ray diffraction.

In the second stage of the reaction, at a critical value of x, close to 0.3, a fraction of the vanadium ions migrates to the octahedral sites of the lithium layer, passing through the tetrahedral interstices.

This transfer causes an adjustment of the lattice to occur, which corresponds to the appearance of phase II, with its characteristic lattice constants.

The migration of vanadium ions from the 3b to the 3a octahedral sites continues until approximately one-third of the vanadium ions occupies the latter. The final product, phase II, is $Li_{1-x}V_{1/3}[V_{2/3}]O_2$, where the square brackets indicate the 3b sites and $x = 0.85 \pm 0.05$.

The apparent two-phase region ($0.3<x<0.85$) is probably due to two factors. Firstly, there may be preferential extraction of lithium from the smaller particles, whilst larger particles of $LiVO_2$ remain unreacted; this phenomenon is known to occur in this type of reaction and has been documented in the case of $Li_{1-x}Mn_2O_4$ [75].

Secondly, it is possible that the vanadium ion transfer takes place faster than the rate at which equilibrium is reached. This would give rise to particles that initially have the lattice constants of phase I. Upon standing at ambient temperature for several weeks, the relative concentration of phase I decreases significantly, whilst phase II increases.

4.5.2 Cyclic voltammetry of $LiVO_2$

Delithiation of $LiVO_2$ was studied by cyclic voltammetry. A typical voltammogram of $LiVO_2$ (scan rate = 1 mV/sec) is shown in Fig. 4.5. The anodic scan confirms the existence of several steps in the delithiation process. The broad peak between 2.70 V and 3.20 V comprises a distinct shoulder at 2.88 V and a well-resolved peak at 3.09 V. A very shallow, broad peak is observed at 3.53 V. The first of these peaks, at 2.88 V, probably corresponds to the removal of approximately one-third of the lithium ions, whilst the vanadium cations remain fixed. The second peak, at 3.09 V, is due to the next step of the reaction, where the extraction of most

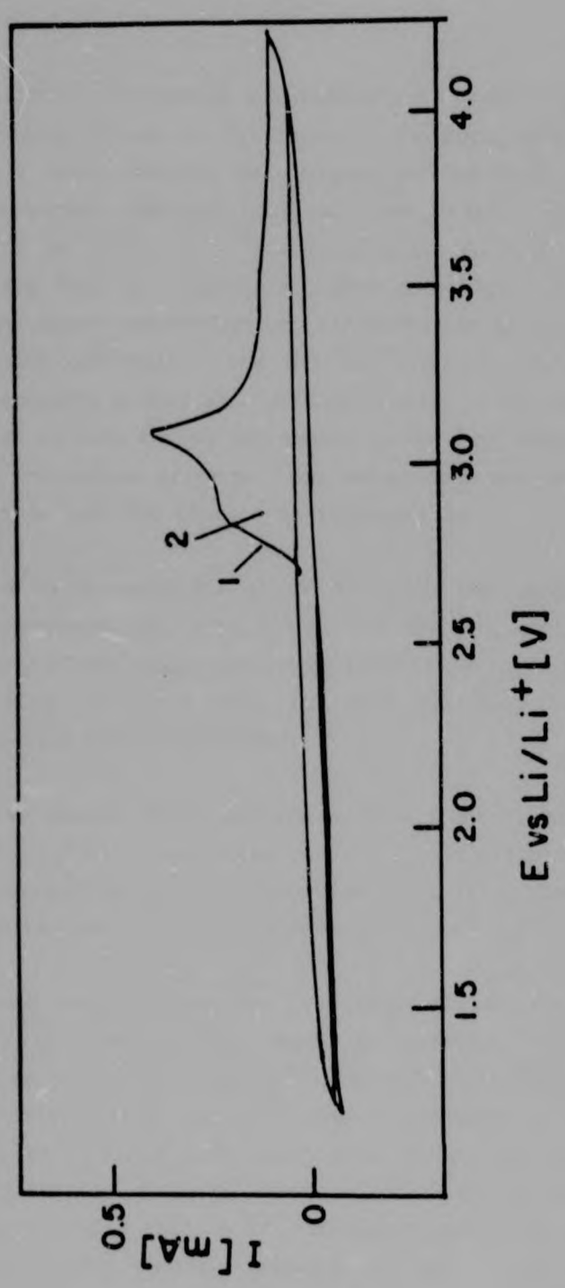

FIG 4.5

Cyclic voltammogram of $LiVO_2$

of the lithium cations is accompanied by a redistribution of the vanadium cations in the layers. The last, shallow peak at 3.53 V could possibly be assigned and the final stage of the extraction, between $Li_{\sim 0.2}VO_2$ and "VO_2". This step could not be achieved by chemical oxidation with bromine, indicating that it requires a higher potential. After the vanadium cation redistribution, Li^+ diffusion is anticipated to be more difficult: the diffuse shape of the peak at 3.53 V suggests a very slow diffusion rate; this would confirm that it does indeed correspond to the last stage of the lithium extraction process. The return scan and subsequent cycles show that the process is irreversible.

In order to investigate at which stage the delithiation becomes irreversible, a fresh cell was scanned, setting progressively higher upper switching potentials for subsequent cycles (Fig. 4.6) and using the same scan rate as in the previous experiment (1 mV/sec).

The first anodic scan, between 2.69 - 2.90 V, shows the shoulder at 2.88 V: upon scan reversal, this process appears to be reversible, with a reduction at 2.73 V, confirming that the layered structure is maintained during this step.

The second cycle, where the imposed upper potential limit was 3.25 V, shows the two oxidation peaks at 2.88 V and 3.12 V, as in the first cycle of Fig. 4.5. Upon scan reversal, a fairly shallow reduction peak is observed, at a voltage of 2.48 V. This would imply that the process at 3.12 V is irreversible, although some relithiation is possible. This subsequent insertion of lithium occurs in a modified structure, where vanadium cations are present in all the layers. Lithiation is therefore anticipated to be slower; this is confirmed by the diffuse aspect of the peak at 2.48 V. The extent of this lithium insertion has been determined chemically: treatment of $Li_{0.28}VO_2$ with n-BuLi led to the composition $Li_{0.9}VO_2$ [140].

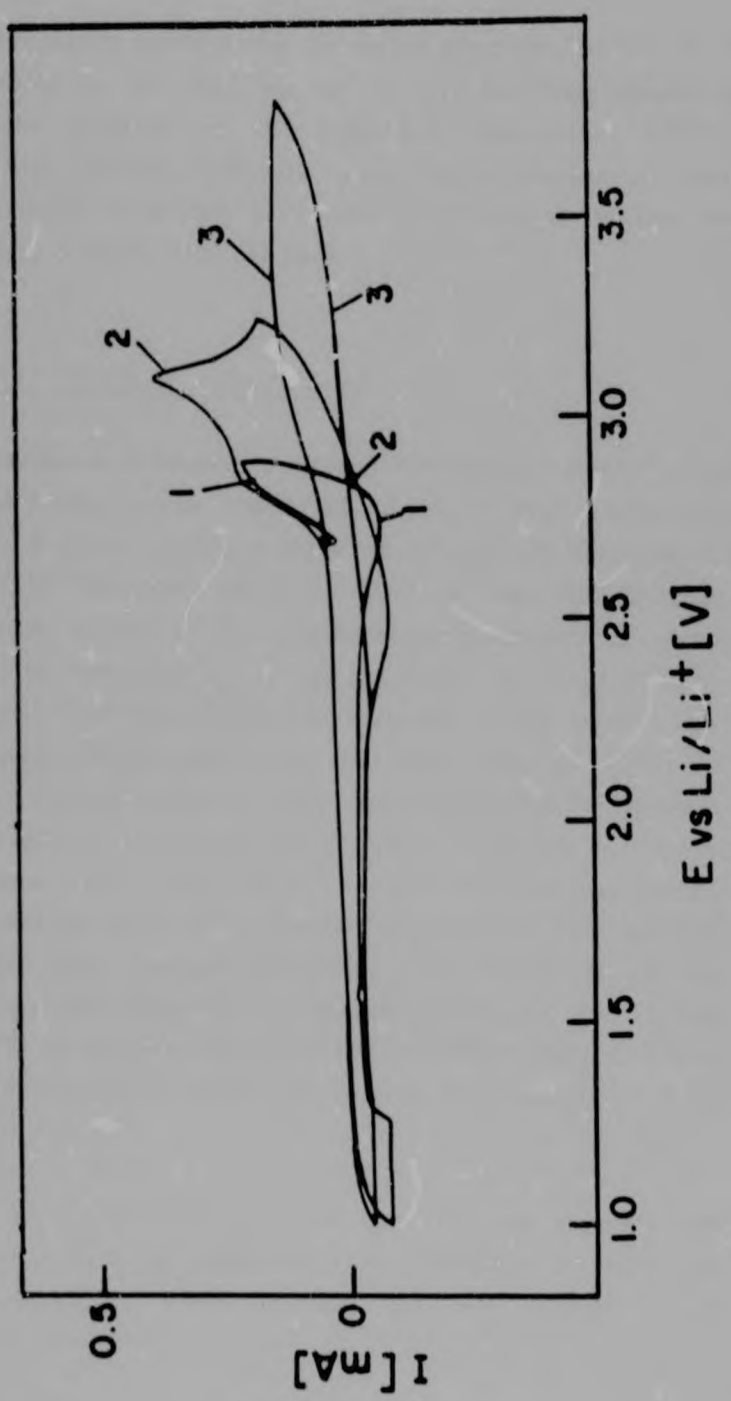

FIG 4.6

Cyclic voltammogram of the system

$Li_{1-x}VO_2$ $(0<x<1)$

The third cycle shows a new oxidation reaction, which can be interpreted as the delithiation of the modified structure, i.e., the reversal of the reduction observed at 2.48 V, during the previous cathodic scan. This process is again characterised by a very slow rate of lithium diffusion, reflected by a wide, shallow peak.

4.5.3 Li^+ diffusion rate in $LiVO_2$

The lithium-ion diffusion rate was determined for the parent compound $LiVO_2$, since the first stage of the delithiation reaction follows a single-phase mechanism (cf Sections 4.3 and 4.5.1). The value of $\tilde{D} = 5.10^{-9}$ cm^2/sec was obtained. Lithium-ion diffusion in intercalation compounds is considered to be fast when it is in the range $10^{-10} < \tilde{D} < 10^{-8}$ cm^2/sec. The Li^+ diffusion rate was measured in the isostructural compound $LiCoO_2$ using both the same technique [141] and another, similar method [142], the galvanostatic intermittent titration technique (GITT, first described by Weppner and Huggins [119]): the value $\tilde{D} = 5.10^{-9}$ cm^2/sec was obtained, suggesting that Li^+ diffusion proceeds at the same rate in the two isostructural compounds, $LiVO_2$ and $LiCoO_2$. A more recent (and more accurate) re-determination of $\tilde{D}$ in Li_xCoO_2 ($0.10 < x < 1$) by Honders et al. [125], showed that, in fact, lithium diffusion in $LiCoO_2$ is considerably faster, with $\tilde{D} = 4.10^{-8}$ cm^2/sec.

The Li^+ diffusion rate obtained here for the layered compound $LiVO_2$ will be compared later (Chapter 6) with the system $Li_{1+x}V_2O_4$, where lithium diffuses through a 3-D network of channels.

4.6 CONCLUSIONS

This study shows that the extraction of lithium from $LiVO_2$ occurs in two stages: initially, for $0 < x < 0.3$ in $Li_{1-x}VO_2$, delithiation

does not provoke any important structural changes and the reaction is reversible. Lithium extraction from the layered parent compound $LiVO_2$ is relatively fast ($\tilde{D} = 5.10^{-9}$ cm^2/sec). In the second stage ($x>0.3$), approximately one-third of the vanadium ions migrates to the octahedral sites of the former lithium layer (3a), passing via the face-sharing tetrahedral sites. This transformation is irreversible. Subsequent re-lithiation proceeds via a different mechanism.

A significant improvement of the R value of the structure refinement of $Li_{0.22}VO_2$ was obtained for several models where vanadium ions occupied the 3a and 3b octahedral and the 6c tetrahedral sites (models 2 - 4, Tables 4.4 - 6). Since vanadium cations would not be stable when occupying face-sharing tetrahedra and octahedra, the latter structure is possible only once a number of octahedral sites have become vacant, due to the progress of the delithiation reaction.

The delithiation mechanisms of the isostructural layered compounds $LiCoO_2$ and $LiNiO_2$ can be compared with that of $LiVO_2$.

In the case of $Li_{1-x}CoO_2$ ($0<x<1$), the structure of the parent compound $LiCoO_2$, where lithium and cobalt cations occupy alternate layers of octahedral sites, is maintained [20]. Recent studies suggest that the cobalt ions remain within the octahedra, but are displaced from the centre [143].

The difference between $Li_{1-x}CoO_2$ and $Li_{1-x}VO_2$ is probably related to the feasibility of the migration through the tetrahedral sites on the part of the transition metal cation.

Although tetravalent vanadium is not commonly found in a tetrahedral environment, it is probable that the V^{4+} ions disproportionate to V^{3+} and V^{5+} (the latter stable in a tetrahedral coordination) prior to the migration. This reaction is known to be ener-

getically accessible [137]. Pentavalent vanadium then migrates via the tetrahedral sites to the 3a sites of the lithium layer.

In the case of the cobalt ion, migration via the tetrahedral sites is more difficult. Tetravalent cobalt, which is a highly oxidising ion, is seldom found in oxides, where it either resides in a tetrahedral or in an octahedral environment; moreover, Co^{4+} ions in tetrahedral sites are observed only in the presence of strong ionic bonding between the oxide anion and other metal cations, such as Li^+, Na^+, K^+, Rb^+, Cs^+ and Ba^{2+} [144]. Therefore in delithiated $Li_{1-x}CoO_2$, where only a little lithium is present, the mainly tetravalent cobalt, which is relatively stable in the octahedral 3b sites, would be unstable in a tetrahedral environment, and is therefore unlikely to migrate via the tetrahedral sites. A disproportionation to Co^{5+} and Co^{3+}, similar to that hypothesised for vanadium, is unlikely, since very few examples of pentavalent cobalt are reported in the literature [136].

Thomas et al. [145] recently reported the formation of $Li_{1-x}NiO_2$ ($x=0.5$), but could not determine its structure due to the line-broadening of the X-ray diffraction pattern.

In the case of $Li_{1-x}NiO_2$, stabilisation of the delithiated compound cannot be achieved by migration of $Ni^{3+/4+}$ cations through the tetrahedral sites, nor through a disproportionation reaction, as both these routes would require considerable energy; furthermore, no energy would be gained by a displacement of nickel ions within the octahedral sites [145].

However, the steps observed in the electrochemical curve of $Li_{1-x}NiO_2$ ($0<x<0.6$) were attributed to a slippage of the sandwich layers relative to one another [145]. This phenomenon was first observed in the layered systems $Na_{1-x}MO_2$ (M = Ti, Cr, Co and Ni) by Delmas et al. [146].

The structural differences between $Li_{1-x}MO_2$ (M = V, Co) compounds are reflected by the cyclic voltammograms of the two systems: delithiation of $LiCoO_2$ has been shown to be reversible [140], whereas lithium extraction from $LiVO_2$ is irreversible.

It is interesting to note that the unit cell of $Li_{0.22}VO_2$, although it remains trigonal, is a lot closer to cubic symmetry than the parent compound, $LiVO_2$. This becomes apparent from a comparison of the X-ray diffraction profiles of $LiVO_2$ and $Li_{0.22}VO_2$ (Figs 4.1, 4.3) : the latter shows a higher degree of symmetry, with some of the reflections merging into one peak. The most characteristic example of this phenomenon is constituted by the {018} and {110} peaks, which are two distinct peaks in $LiVO_2$, and overlap almost entirely in $Li_{0.22}VO_2$. The anion positional parameter, z, of $Li_{0.22}VO_2$ refines to 0.249(1), far closer to the cubic value of 0.250 than $LiVO_2$, where z=0.239 [134].

This gradual change of symmetry, which is not yet complete in $Li_{0.22}VO_2$, could facilitate the transformation of $Li_{0.5}VO_2$ to the cubic spinel LiV_2O_4. This conversion will be described in the following chapter.

CHAPTER 5

THE TRANSFORMATION OF DELITHIATED $LiVO_2$ INTO THE SPINEL STRUCTURE

5.1 INTRODUCTION

The spinel LiV_2O_4 was first prepared by Reuter and Jaskowsky in 1950 [147], and has since been obtained by one of the following high-temperature syntheses:

$$a)\quad Li_2O + V_2O_3 + 2VO_2 \xrightarrow[700 - 750\ ^\circ C]{\text{Vacuum}} 2LiV_2O_4 \qquad [147]$$

$$b)\quad Li_2CO_3 + V_2O_3 + 2VO_2 \xrightarrow[700 - 750\ ^\circ C]{\text{Vacuum}} 2LiV_2O_4 + CO_2 \qquad [148]$$

$$c)\quad LiVO_2 + VO_2 \xrightarrow[700 - 750\ ^\circ C]{\text{Vacuum}} LiV_2O_4 \qquad [149]$$

These methods of preparation are delicate because of the volatility of Li_2O and because of the strong tendency of V^{4+} to oxidise to V^{5+}, forming V_2O_5.

Attempts to prepare pure LiV_2O_4 reproducibly by any of these methods were unsuccessful in this laboratory, confirming the observations of other workers [150].

This difficulty prompted the investigation of a new pathway to prepare LiV_2O_4, by analogy with the method used by Murphy et al. [77] for the synthesis of $LiTi_2O_4$, where partly lithiated anatase $Li_{0.5}TiO_2$ was converted to spinel by annealing at ~700 °C.

CHAPTER 5

THE TRANSFORMATION OF DELITHIATED $LiVO_2$ INTO THE SPINEL STRUCTURE

5.1 INTRODUCTION

The spinel LiV_2O_4 was first prepared by Reuter and Jaskowsky in 1950 [147], and has since been obtained by one of the following high-temperature syntheses:

$$\text{a)}\quad Li_2O + V_2O_3 + 2VO_2 \xrightarrow[700 - 750\,^{\circ}C]{\text{Vacuum}} 2LiV_2O_4 \qquad [147]$$

$$\text{b)}\quad Li_2CO_3 + V_2O_3 + 2VO_2 \xrightarrow[700 - 750\,^{\circ}C]{\text{Vacuum}} 2LiV_2O_4 + CO_2 \qquad [148]$$

$$\text{c)}\quad LiVO_2 + VO_2 \xrightarrow[700 - 750\,^{\circ}C]{\text{Vacuum}} LiV_2O_4 \qquad [149]$$

These methods of preparation are delicate because of the volatility of Li_2O and because of the strong tendency of V^{4+} to oxidise to V^{5+}, forming V_2O_5.

Attempts to prepare pure LiV_2O_4 reproducibly by any of these methods were unsuccessful in this laboratory, confirming the observations of other workers [150].

This difficulty prompted the investigation of a new pathway to prepare LiV_2O_4, by analogy with the method used by Murphy et al. [77] for the synthesis of $LiTi_2O_4$, where partly lithiated anatase $Li_{0.5}TiO_2$ was converted to spinel by annealing at ~700 °C.

In this chapter, the transformation of the compounds $Li_{0.50}VO_2$ and $Li_{0.45}VO_2$ into the spinels LiV_2O_4 and $Li_{0.90}V_2O_4$ respectively is described, and a structure analysis of the products is reported.

5.2 EXPERIMENTAL

Samples with the composition $Li_{\sim 0.5}VO_2$ were prepared by bromine oxidation of $LiVO_2$, using stoichiometric quantities of bromine, as described in section 3.2.1 and 4.2.

The compounds $Li_{0.50}VO_2$ and $Li_{0.45}VO_2$ were sealed under vacuum in a pyrex glass tube, and heated at a temperature of 300°C for periods ranging from 54 to 100 hours. After rapid cooling, a black powder was obtained.

Differential scanning calorimetry (DSC) experiments were performed as detailed in section 3.5 on a sample with the composition $Li_{0.45}VO_2$.

5.3 RESULTS

The stoichiometry $Li_{0.50}VO_2$ is difficult to obtain with precision due to the experimental error in the concentration of the bromine solution, and because of the slight lithium deficiency sometimes encountered in $LiVO_2$.

For this reason several samples were prepared, using different quantities of bromine; their lithium content was analysed by atomic absorption spectroscopy.

Samples with the composition Li_xVO_2, where x=0.37, 0.41, 0.45 and 0.50 were heated to 300 °C and X-rayed at ambient temperature.

The powder X-ray diffraction profiles were characteristic of the cubic spinels, which crystallise in the cubic space-group Fd3m.

After heat-treatment, the X-ray patterns of the samples with a low lithium content, derived from $Li_{0.37}VO_2$ and $Li_{0.41}VO_2$, showed relatively broad peaks, and contained a small amount of VO_2 and V_2O_3.

The compounds derived from $Li_{0.45}VO_2$ and $Li_{0.50}VO_2$ had better resolved peaks, and appeared to be almost single-phase, except for trace amounts of impurities, most of which could be identified as VO_2. Representative X-ray diffraction patterns of $Li_{0.9}V_2O_4$ and $Li_{1.0}V_2O_4$ are given in Figs 5.1 - 2. Interplanar spacings and relative intensities for the two compounds are given in Tables 5.1 - 2.

In all cases the X-ray diffraction patterns could be indexed to a cubic unit cell : the lattice constant of $Li_{1.0}V_2O_4$ (a=8.241(1)Å) was in good agreement with that reported in the literature (a=8.240(1)Å) [151]. The lattice constant obtained for $Li_{0.9}V_2O_4$ (a = 8.244(1)Å) is slightly larger.

Spinels obtained from starting materials with the composition $Li_{0.41}VO_2$ and $Li_{0.37}VO_2$ had substantially the same lattice parameter as $Li_{0.9}V_2O_4$, but were contaminated with increasing amounts of VO_2 and V_2O_3, suggesting that the limiting composition of the cation-deficient spinel is approximately $Li_{0.9}V_2O_4$.

The relative intensities of the spinel peaks in all the patterns were very similar.

The X-ray powder diffraction profile of a sample of LiV_2O_4 prepared at high temperature (method c, cf section 5.1) is given in Fig. 5.3; most of the impurity peaks in the pattern could be identified as Li_3VO_4. A comparison of the profiles of the two samples prepared from the conversion of $Li_{\sim 0.5}VO_2$ with LiV_2O_4 obtained from the more conventional high temperature synthesis, shows a marked difference in the distribution of the relative intensities of the reflections.

The powder X-ray diffraction profiles were characteristic of the cubic spinels, which crystallise in the cubic space-group Fd3m.

After heat-treatment, the X-ray patterns of the samples with a low lithium content, derived from $Li_{0.37}VO_2$ and $Li_{0.41}VO_2$, showed relatively broad peaks, and contained a small amount of VO_2 and V_2O_3.

The compounds derived from $Li_{0.45}VO_2$ and $Li_{0.50}VO_2$ had better resolved peaks, and appeared to be almost single-phase, except for trace amounts of impurities, most of which could be identified as VO_2. Representative X-ray diffraction patterns of $Li_{0.9}V_2O_4$ and $Li_{1.0}V_2O_4$ are given in Figs 5.1 - 2. Interplanar spacings and relative intensities for the two compounds are given in Tables 5.1 - 2.

In all cases the X-ray diffraction patterns could be indexed to a cubic unit cell : the lattice constant of $Li_{1.0}V_2O_4$ (a=8.241(1)Å) was in good agreement with that reported in the literature (a=8.240(1)Å) [151]. The lattice constant obtained for $Li_{0.9}V_2O_4$ (a = 8.244(1)Å) is slightly larger.

Spinels obtained from starting materials with the composition $Li_{0.41}VO_2$ and $Li_{0.37}VO_2$ had substantially the same lattice parameter as $Li_{0.9}V_2O_4$, but were contaminated with increasing amounts of VO_2 and V_2O_3, suggesting that the limiting composition of the cation-deficient spinel is approximately $Li_{0.9}V_2O_4$.

The relative intensities of the spinel peaks in all the patterns were very similar.

The X-ray powder diffraction profile of a sample of LiV_2O_4 prepared at high temperature (method c, cf section 5.1) is given in Fig. 5.3; most of the impurity peaks in the pattern could be identified as Li_3VO_4. A comparison of the profiles of the two samples prepared from the conversion of $Li_{\sim 0.5}VO_2$ with LiV_2O_4 obtained from the more conventional high temperature synthesis, shows a marked difference in the distribution of the relative intensities of the reflections.

In particular, the ratios $\frac{I\{400\}}{I\{111\}}$ and $\frac{I\{311\}}{I\{111\}}$ are drastically changed.

Significant differences of this type are generally indicative of an unusual distribution of the cations within the lattice : an intensity refinement of the X-ray powder diffraction pattern was undertaken, in order to better understand the structures obtained.

TABLE 5.1

X-ray diffraction pattern of $Li_{0,9}V_2O_4$

Space group : Fd3m a=8.244(1)Å α=90°

hkl	d^{*}_{obs} [Å]	d_{calc} [Å]	I^{**}_{obs}
111	4.756	4.760	1000
311	2.486	2.486	726
222	2.382	2.380	96
400	2.062	2.061	935
331	1.892	1.891	94
511	1.586	1.587	247
333	1.586	1.587	
440	1.457	1.457	558
531	1.392	1.394	139
533	1.257	1.257	67
622	-	1.243	54
444	1.190	1.190	112
551	1.155	1.154	72
711	1.155	1.154	
553	1.073	1.073	92
731	1.073	1.073	
800	1.030	1.031	69
751	0.952	0.952	
555	0.952	0.952	110
662	-	0.946	
840	0.922	0.922	180
753	0.904	0.905	
911	0.904	0.905	79
842	-	0.900	

* No d_{obs} is indicated for weak and diffuse peaks

** I_{obs} normalised to 1000

TABLE 5.2

X-ray diffraction pattern of $Li_{1.0}V_2O_4$

Space group : Fd3m a=8.241(1)Å α=90°

hkl	d_{obs}* [Å]	d_{calc} [Å]	I_{obs}**
111	4.772	4.758	1000
311	2.487	2.485	609
222	2.381	2.379	88
400	2.063	2.060	863
331	1.891	1.891	91
511	1.585	1.586	187
333	1.585	1.586	
440	1.455	1.457	506
531	1.393	1.393	143
533	1.256	1.257	113
622	1.243	1.243	
444	1.190	1.190	112
551	1.154	1.154	61
711	1.154	1.154	
553	1.072	1.073	74
731	1.072	1.073	
800	-	1.030	68
751	-	0.952	107
555	-	0.952	
662	-	0.945	173
840	0.922	0.921	
753	-	0.905	77
911	-	0.905	
842	-	0.899	

* No d_{obs} is indicated for weak and diffuse peaks

** I_{obs} normalised to 1000

5.4 STRUCTURE OF $Li_{0.9}V_2O_4$ AND $Li_{1.0}V_2O_4$

5.4.1 Structural characterisation

Structure determinations of $Li_{0.9}V_2O_4$ and $Li_{1.0}V_2O_4$ prepared from $Li_{0.45}VO_2$ and $Li_{\sim 0.5}VO_2$ respectively were undertaken by an intensity refinement of the various peaks of the powder X-ray diffraction patterns (Figs 5.1 - 2), using 17 and 16 intensities respectively, which corresponded to 24 reflections.

In the first attempt to refine the structures, the compounds $Li_xV_2O_4$ were assumed to have the structure of $Li[V_2]O_4$, i.e., that of a normal spinel where Li^+ occupies the tetrahedral 8a sites, and the $V^{4+/3+}$ ions are situated in the octahedral 16d sites [151].

The site occupancies were kept constant, with the values defined by the formulae $Li_{0.9}[V_2]O_4$ and $Li_{1.0}[V_2]O_4$. B_{iso} of the lithium ions was fixed at $1.0Å^2$.

The isotropic temperature factors of the vanadium and the oxide ions were allowed to vary, as were the fractional coordinates (defining the u parameter) of the anion O^{2-}.

This model (model 1) gave R=12.2% in the case of $Li_{0.9}V_2O_4$ and 8.9% for $Li_{1.0}V_2O_4$.

The structural parameters of both compounds, as obtained according to model 1 are listed in Tables 5.3a and 5.4a, the observed and calculated intensities in Tables 5.3b and 5.4b.

The calculated intensities of some of the larger peaks differ quite considerably from the observed. This is particularly true for the {111} and {311} reflections of $Li_{0.9}V_2O_4$, where the ratio $\frac{I_{calc}\{311\}}{I_{calc}\{111\}} = 0.55$ is significantly smaller than the ratio $\frac{I_{obs}\{311\}}{I_{obs}\{111\}} = 0.73$.

TABLE 5.3a

Structural parameters of $Li_{0.9}[V_2]O_4$ (model 1)

R = 12.2 %

Space group : $Fd3m$ (O_h^7) a = 8.244(1)Å

ATOM	POSITION	x	y	z	B[Å^2]	n
Li^+	8a	0.125	0.125	0.125	1.0	0.9
$V^{3+/4+}$(*)	16d	0.500	0.500	0.500	0.02(30)	2.0
O^{2-}	32e	0.257(2)	0.257(2)	0.257(2)	1.7(8)	4.0

* Mean oxidation state of vanadium : 3.55

TABLE 5.3b

Observed and calculated intensities for $Li_{0.9}V_2O_4$ (model 1)

hkl	I_{obs}	I_{calc}	hkl	I_{obs}	I_{calc}
111	926	1021	551 }	67	76
311	672	558	711 }		
222	89	32	553 }	85	90
400	866	825	731 }		
331	87	138	800	64	56
511 }	229	211	751 }		
333 }			555 }	102	111
440	517	445	662 }		
531	129	148	840	167	171
533	59	54	753 }		
622	61	51	911 }	73	72
444	105	110	842 }		

TABLE 5.4a

Structural parameters of $Li[V_2]O_4$ (model 1)

R = 8.9 %

Space group : $Fd3m$ (O_h^7) a = 8.241(1)Å

ATOM	POSITION	x	y	z	B[Å^2]	n
Li^+	8a	0.125	0.125	0.125	1.0	1.0
$V^{3+/4+}$(*)	16d	0.500	0.500	0.500	0.1(3)	2.0
O^{2-}	32e	0.258(2)	0.258(2)	0.258(2)	1.4(7)	4.0

* Mean oxidation state of vanadium : 3.50

TABLE 5.4b

Observed and calculated intensities for $Li[V_2]O_4$ (model 1)

hkl	I_{obs}	I_{calc}	hkl	I_{obs}	I_{calc}
111	985	1027	551 }	60	75
311	600	550	711 }		
222	87	30	553 }	72	86
400	851	814	731 }		
331	90	125	800	67	56
511 }	184	216	751 }		
333 }			555 }	105	106
440	498	445	662 }		
531	141	146	840	170	169
533 }	111	99	753 }		
622 }			911 }	76	70
444	110	109	842 }		

The relative intensities of the {111} and {311} reflections of spinels are generally indicative of the nature of the atoms residing on the tetrahedral 8a sites (cf Appendix).

It can be calculated from the contribution of the various atoms to the intensity of a particular reflection that the {111} peak is usually very intense if the 8a positions are occupied by light atoms, as in $Li[Mn_2]O_4$ and $Li[Ti_2]O_4$ [152,153]. This reflection is a lot weaker when the A cation is a relatively heavy atom; in this case, the {311} reflection is usually the strongest peak, as in Fe_3O_4, $LiFe_5O_8$ and $CoCr_2O_4$ [154-156].

In view of this observation, the difference between the observed and calculated ratios $\frac{I\{311\}}{I\{111\}}$ for $Li_{0.9}V_2O_4$ would suggest the presence of relatively heavy vanadium ions in the 8a sites.

In model 2, the vanadium ions were allowed to occupy both the tetrahedral 8a sites and the octahedral 16d sites, whilst the lithium content remained fixed in the 8a sites with the values obtained by atomic absorption analysis.

TABLE 5.4b

Observed and calculated intensities for $Li[V_2]O_4$ (model 1)

hkl	I_{obs}	I_{calc}	hkl	I_{obs}	I_{calc}
111	985	1027	551 }	60	75
311	600	550	711 }		
222	87	30	553 }	72	86
400	851	814	731 }		
331	90	125	800	67	56
511 }	184	216	751 }		
333 }			555 }	105	106
440	498	445	662 }		
531	141	146	840	170	169
533 }	111	99	753 }		
622 }			911 }	76	70
444	110	109	842 }		

The relative intensities of the {111} and {311} reflections of spinels are generally indicative of the nature of the atoms residing on the tetrahedral 8a sites (cf Appendix).

It can be calculated from the contribution of the various atoms to the intensity of a particular reflection that the {111} peak is usually very intense if the 8a positions are occupied by light atoms, as in $Li[Mn_2]O_4$ and $Li[Ti_2]O_4$ [152,153]. This reflection is a lot weaker when the A cation is a relatively heavy atom; in this case, the {311} reflection is usually the strongest peak, as in Fe_3O_4, $LiFe_5O_8$ and $CoCr_2O_4$ [154-156].

In view of this observation, the difference between the observed and calculated ratios $\frac{I\{311\}}{I\{111\}}$ for $Li_{0.9}V_2O_4$ would suggest the presence of relatively heavy vanadium ions in the 8a sites.

In model 2, the vanadium ions were allowed to occupy both the tetrahedral 8a sites and the octahedral 16d sites, whilst the lithium content remained fixed in the 8a sites with the values obtained by atomic absorption analysis.

In the course of the refinement, the vanadium occupancies in 8a and 16d, the B_{iso} factors of the vanadium in 16d and of the oxide ion, and the anion fractional coordinates were allowed to vary.

The B_{iso} factors of the lithium ions and of the vanadium ions in 8a were kept constant at $1.0Å^2$ and $0.5Å^2$ respectively.

In the case of $Li_{0.9}V_2O_4$ the final R value, viz. 7.3%, obtained with model 2, was a meaningful improvement over model 1 (R=12.2%). Furthermore, with this model, the ratio $\frac{I_{calc}\{311\}}{I_{calc}\{111\}}$ = 0.68 is significantly closer to the observed value (viz. 0.73) than in the case of model 1.

This refinement gave a vanadium occupancy of 0.09(3) in the 8a sites and 1.91(3) in the 16d sites. Assuming all the lithium ions are located in the tetrahedral sites, and within experimental error, this implies that the 8a sites are fully occupied, and 5% of the 16d sites are vacant as in $Li_{0.9}V_{0.1}[V_{1.9}\square_{0.1}]O_4$.

The full atomic parameters of $Li_{0.9}V_2O_4$ for model 2 are given in Table 5.5a, the observed and calculated intensities in Table 5.5b.

Although model 1 yielded a relatively good fit for $Li_{1.0}V_2O_4$ (R=8.9%), a further refinement according to model 2 was carried out, using the same conditions as for $Li_{0.9}V_2O_4$.

In this case, the refined vanadium occupancies amounted to 1.97(3) and 0.03(3) in the 16d and 8a sites respectively.

The R value of 7.6% indicated that model 2 could be a slight improvement over model 1, but showed within experimental error the normal spinel distribution. The full structural parameters of $Li_{1.0}V_2O_4$ according to model 2 are given in Table 5.6a, the observed and calculated intensities in Table 5.6b.

TABLE 5.5a

Structural parameters of $Li_{0.9}V_2O_4$ (mr ?)

R = 7.3 %

Space group : Fd3m (O_h^7) a = 8.244(1)Å

ATOM*	POSITION	x	y	z	B[Å^2]	n
Li^+	8a	0.125	0.125	0.125	1.0	0.9
V^{5+}	8a	0.125	0.125	0.125	0.5	0.09(3)
$V^{3+/4+}$	16d	0.500	0.500	0.500	0.1(2)	1.91(3)
O^{2-}	32e	0.258(2)	0.258(2)	0.258(2)	1.9(7)	4.0

* Mean oxidation state of vanadium: 3.55

TABLE 5.5b

Observed and calculated intensities for $Li_{0.9}V_2O_4$ (model 2)

hkl	I_{obs}	I_{calc}	hkl	I_{obs}	I_{calc}
111	926	960	551 }	67	68
311	672	653	711 }		
222	89	25	553 }	85	101
400	866	823	731 }		
331	87	109	800	64	60
511 }	229	250	751 }		
333 }			555 }	102	120
440	517	489	662 }		
531	129	133	840	167	155
533	59	62	753 }		
622	61	50	911 }	73	63
444	105	104	842 }		

TABLE 5.6a

Structural parameters of $Li_{1.0}V_2O_4$ (model 2)

R = 7.6 %

Space group : Fd3m (O_h^7) a = 8.241(1)Å

ATOM*	POSITION	x	y	z	B[Å^2]	n
Li^+	8a	0.125	0.125	0.125	1.0	1.0
V^{5+}	8a	0.125	0.125	0.125	0.5	0.03(3)
$V^{3+/4+}$	16d	0.500	0.500	0.500	0.1(3)	1.97(3)
O^{2-}	32e	0.258(2)	0.258(2)	0.258(2)	1.5(7)	4.0

* Mean oxidation state of vanadium: 3.50

TABLE 5.6b

Observed and calculated intensities for $Li_{1.0}V_2O_4$ (model 2)

hkl	I_{obs}	I_{calc}	hkl	I_{obs}	I_{calc}
111	985	1003	551 }	60	72
311	600	579	711 }		
222	87	27	553 }	72	90
400	851	813	731 }		
331	90	115	800	67	57
511 }	184	228	751 }		
333 }			555 }	105	108
440	498	459	662 }		
531	141	140	840	170	164
533 }	111	101	753 }		
622 }			911 }	76	66
444	110	107	842 }		

5.4.2 Discussion

Although the lattice constant and the anion positional parameter of the spinel obtained were consistent with those available in the literature for LiV_2O_4 (a=8.240(1)Å, u=0.260) [151], the intensity distribution of the powder X-ray diffraction pattern seemed to indicate a different cation distribution from that of the normal spinel $Li[V_2]O_4$.

Intensity refinements, which were carried out on two compounds, $Li_{0.9}V_2O_4$ and $Li_{1.0}V_2O_4$, gave an improved fit when the vanadium ions were allowed to occupy both the octahedral 16d sites, as in the normal spinel $Li[V_2]O_4$, and the tetrahedral 8a sites (model 2).

In the case of the lithium-deficient spinel $Li_{0.9}V_2O_4$, the refinement gave 0.09(3) vanadium ions in the 8a sites, whereas in $Li_{1.0}V_2O_4$ the 8a sites appeared to contain scarcely any vanadium ions, with a refined occupancy of 0.03(3).

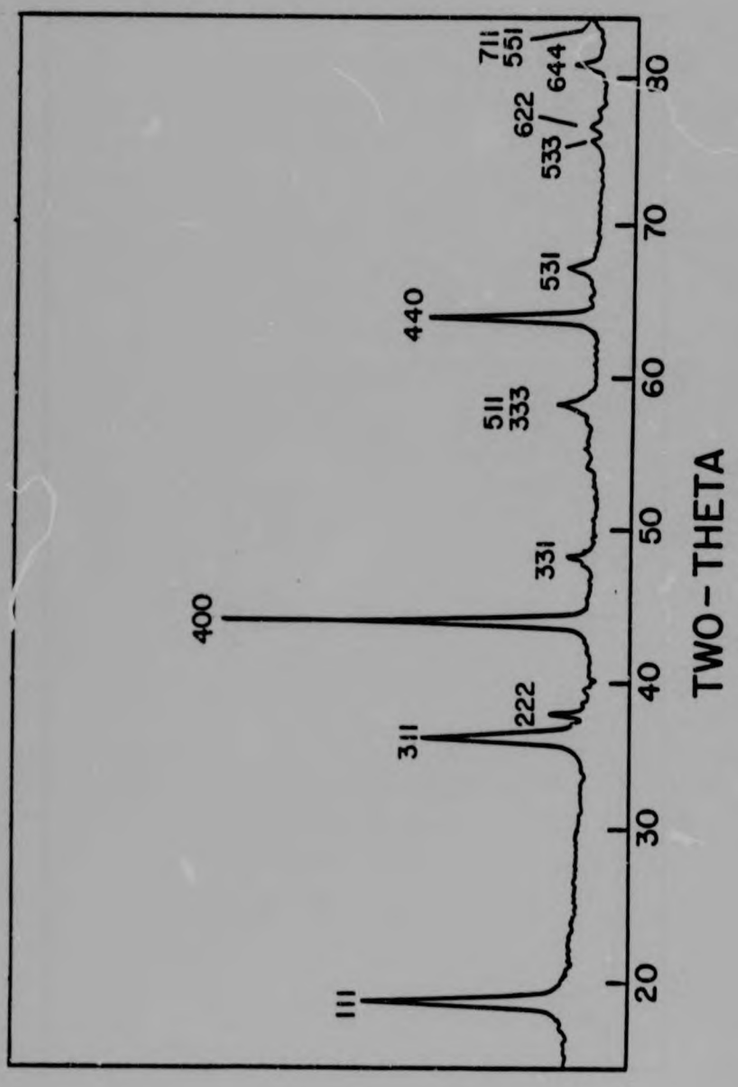

FIG 5.1
X-ray diffraction pattern of $Li_{0.9}V_2O_4$

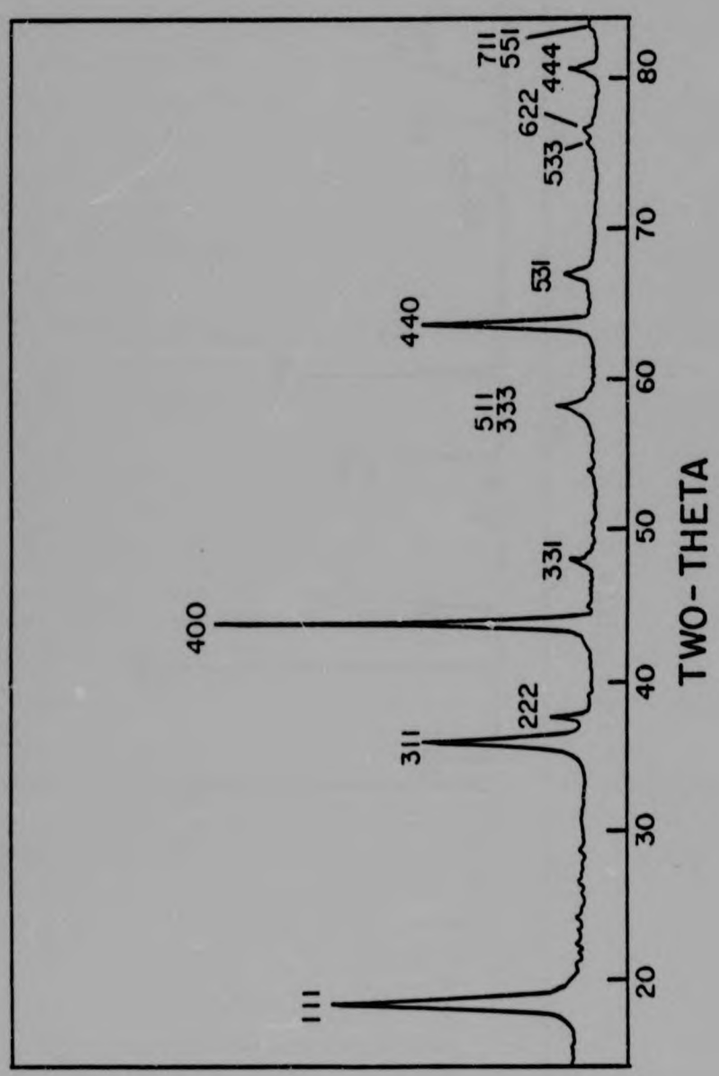

FIG 5.2
X-ray diffraction pattern of $Li_{1.0}V_2O_4$

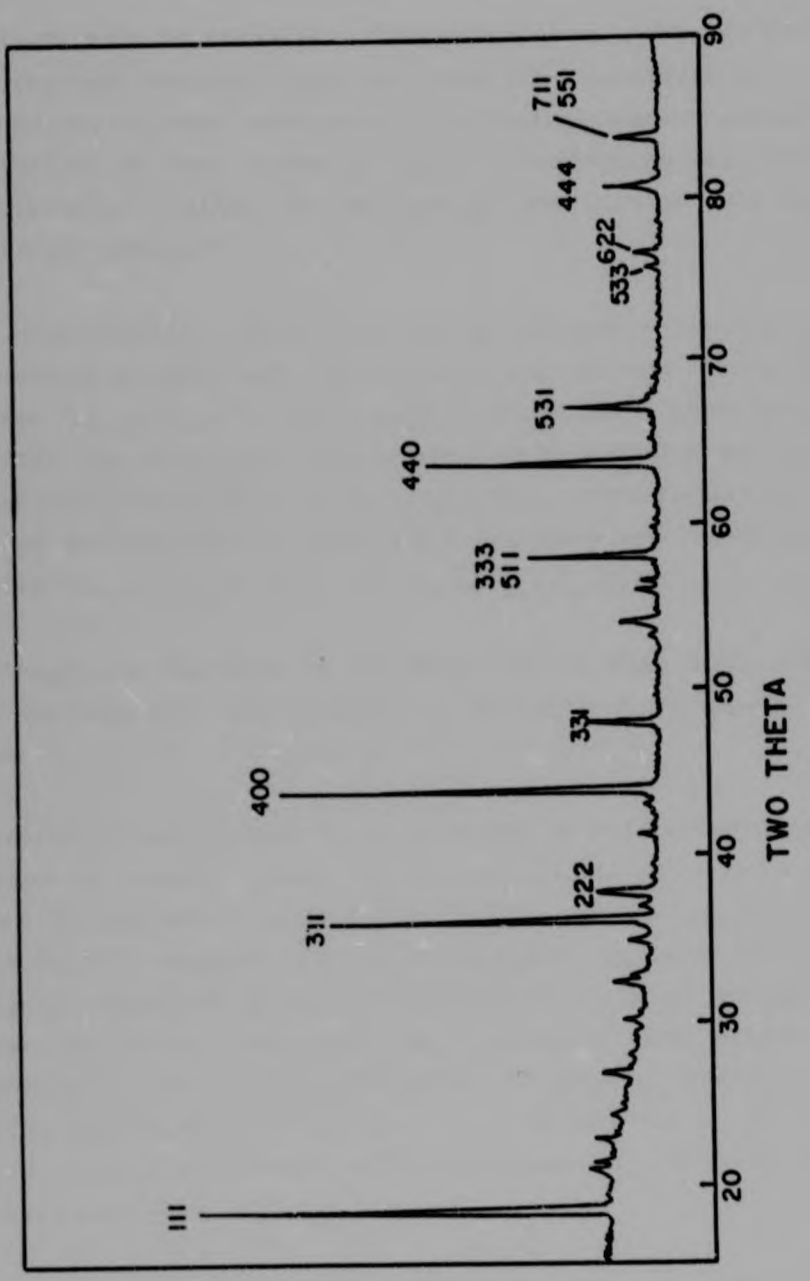

FIG 5.3
X-ray diffraction pattern of LiV_2O_4 (high temperature synthesis)

All attempts to refine the lithium occupancy proved futile, due to the fact that this atom is a very light scatterer of X-rays, in particular when compared to the heavier vanadium atoms. The structure of these compounds cannot therefore be described unequivocally, since the position of the lithium ions is not entirely certain.

Several possible structures can be suggested for $Li_{0.9}V_2O_4$: structure A, where all the available lithium ions occupy the 8a sites ($Li_{0.91}V_{0.09}[V_{1.91}\square_{0.09}]O_4$), structure B, where the octahedral 16d sites are entirely occupied by vanadium and lithium ions ($Li_{0.81}V_{0.09}\square_{0.10}[Li_{0.09}V_{1.91}]O_4$), and structure C, where there are vacancies in both the tetrahedral and the octahedral sites ($Li_{0.91-x}V_{0.09}\square_x[Li_xV_{1.91}\square_{0.09-x}]O_4$).

Although on the basis of our data, none of these structures can be entirely excluded, structure A is favoured for several reasons.

Firstly, there appears to be a strong correlation between the amount of vanadium present in the tetrahedral sites and the extent of the cation deficiency: in the case of $Li_{0.9}V_2O_4$ there are 0.09(3) vanadium ions in the 8a positions, which would fill all the vacant 8a sites, within experimental error and assuming that the lithium ions occupy the tetrahedral sites exclusively. Conversely, in $Li_{1.0}V_2O_4$ the number of vanadium ions in the 8a sites amounts to 0.03(3) and could compensate for a very slight lithium deficiency, which might have remained undetected by the atomic absorption analysis.

The proportion of vanadium ions present in the 8a sites thus decreases as the lithium content approaches 1.0: if all the lithium ions occupy the tetrahedral 8a sites, this observation would support the choice of a structure where all the tetrahedral sites must be filled.

This argument is further supported by Rousset and co-workers [157], who maintain that vacant tetrahedral sites are most unusual in cation-deficient, oxo-spinels, which generally exhibit octahedral vacancies, as in γ-Fe_2O_3 ($Fe_3[Fe_5\square]O_{12}$) [44] and $Zn_2[Ge_3\square]O_8$ [158], whereas tetrahedral vacancies are commonly found in cation-deficient sulfospinels, e.g., in β-In_2S_3 [159].

A preference for octahedral vacancies in oxo-spinels is also noted by Laqua et al. [160].

Moreover, the preparation of cation-deficient spinels with vacant tetrahedral sites appears to be extremely complex: several substituted cation-deficient iron spinels with this structure were recently obtained by a process of selective substitution followed by oxidation [157].

Lastly, the reaction of MgO and V_2O_3 in a reducing atmosphere yields a metastable magnesium vanadium spinel, which is reported to have octahedral vacancies [161]. This further confirms the propensity of cation-deficient oxo-spinels to form vacancies in the octahedral sites rather than in the tetrahedral sites.

It thus seems likely that the cation-deficient $Li_{1-x}V_2O_4$ would prefer structure A, with vacancies in the octahedral sites, i.e., $Li_{1-x}V_x[V_{2-x}\square_x]O_4$.

As in the case of $Li_{0.22}VO_2$, the presence of vanadium ions with tetrahedral coordination raises the question of their oxidation state. As it has already been stated in section 4.6, vanadium ions are usually found to be pentavalent in a tetrahedral environment. Although further proof would be necessary to verify this statement, it may be hypothesised that, as in the case of $Li_{0.22}VO_2$ (section 4.4.7), the spinel $Li_yV_2O_4$ ($0.9<y<1.0$) contains V^{5+} in the tetrahedral 8a sites and $V^{3+/4+}$ in the octahedral 16d sites. The final structure of these metastable spinels would thus be:

$$Li_{1-x}\ V_x^{5+}\ [V_{2-x}^{3+/4+}\square_x]O_4$$

in which three oxidation states of vanadium, V^{3+}, V^{4+} and V^{5+} coexist within one crystal lattice.

5.5 DSC STUDY OF THE CONVERSION OF $Li_{\sim 0.45}VO_2$ TO $Li_{\sim 0.9}V_2O_4$

The transformation of the two-phase layered $Li_{0.45}VO_2$ to the cubic spinel $Li_{0.9}V_2O_4$ was examined by differential scanning calorimetry (DSC).

The conversion takes place in two stages, which can be observed by the DSC technique.

Several samples were heated to different temperatures before and after the transitions and then rapidly quenched to room temperature. The structure of these samples was characterised by powder X-ray diffraction.

The X-ray diffraction pattern of the starting material is given in Fig 4.2; the structure of this compound is discussed in section 4.3.

Two weakly defined, irreversible endothermic transitions are observed at approximately 250 °C and 300 °C (Fig 5.4a). On heating, prior to the first transition, the two-phase character of the starting material persists; however, the relative intensities of the X-ray diffraction patterns indicate a decrease of phase I and a simultaneous increase of phase II.

Furthermore, the pattern of phase II becomes sharper; the gradual merging of some of the peaks, in particular of the {018} and {110} reflections, shows that the lattice approaches cubic symmetry to a greater extent than prior to the heat treatment.

During the first transition, at ~250 °C, phase I disappears entirely; the remaining phase, which strongly resembles the heat-treated phase II, displays quasi-cubic symmetry, although it can be indexed to the trigonal space group $R\bar{3}m$, with the lattice constants a=2.904(1)Å and c=14.287(7)Å.

The intensity distribution of the reflections is similar to that of the delithiated compound $Li_{0.22}VO_2$. This suggests that a significant proportion of the vanadium ions is situated in the layer which was previously occupied solely by lithium ions in $LiVO_2$.

From the X-ray and DSC data it appears that phase I is constituted by particles of the composition $Li_{1-x}VO_2$ with various x. The most delithiated particles of this phase convert to phase II at a relatively low temperature, as very little activation energy is required for the migration of the vanadium ions from one layer to the next. This conversion possibly occurs over a fairly wide range of temperature, and remains undetected by DSC.

The remaining particles, of a composition closer to $LiVO_2$, are more stable, and maintain the original cation distribution of lithium and vanadium in alternate layers up to T=250 °C. At this temperature a solid state reaction occurs, which completes the transformation of phase I into phase II, and the system reaches equilibrium.

The second transition, which takes place at ~300 °C, is the transformation of the quasi-cubic phase to the cubic spinel, $Li_{0.9}V_2O_4$. This conversion occurs through the migration of lithium and vanadium ions through the face-sharing tetrahedral and octahedral interstitial sites.

In the trigonal phase, obtained at 250 °C, the ratio of the vanadium cations in the successive layers is 2:1, as in $Li_{0.2}VO_2$. In the spinel structure, this ratio is 3:1.

During the first transition, at ~250 °C, phase I disappears entirely; the remaining phase, which strongly resembles the heat-treated phase II, displays quasi-cubic symmetry, although it can be indexed to the trigonal space group $R\bar{3}m$, with the lattice constants a=2.904(1)Å and c=14.287(7)Å.

The intensity distribution of the reflections is similar to that of the delithiated compound $Li_{0.22}VO_2$. This suggests that a significant proportion of the vanadium ions is situated in the layer which was previously occupied solely by lithium ions in $LiVO_2$.

From the X-ray and DSC data it appears that phase I is constituted by particles of the composition $Li_{1-x}VO_2$ with various x. The most delithiated particles of this phase convert to phase II at a relatively low temperature, as very little activation energy is required for the migration of the vanadium ions from one layer to the next. This conversion possibly occurs over a fairly wide range of temperature, and remains undetected by DSC.

The remaining particles, of a composition closer to $LiVO_2$, are more stable, and maintain the original cation distribution of lithium and vanadium in alternate layers up to T=250 °C. At this temperature a solid state reaction occurs, which completes the transformation of phase I into phase II, and the system reaches equilibrium.

The second transition, which takes place at ~300 °C, is the transformation of the quasi-cubic phase to the cubic spinel, $Li_{0.9}V_2O_4$. This conversion occurs through the migration of lithium and vanadium ions through the face-sharing tetrahedral and octahedral interstitial sites.

In the trigonal phase, obtained at 250 °C, the ratio of the vanadium cations in the successive layers is 2:1, as in $Li_{0.2}VO_2$. In the spinel structure, this ratio is 3:1.

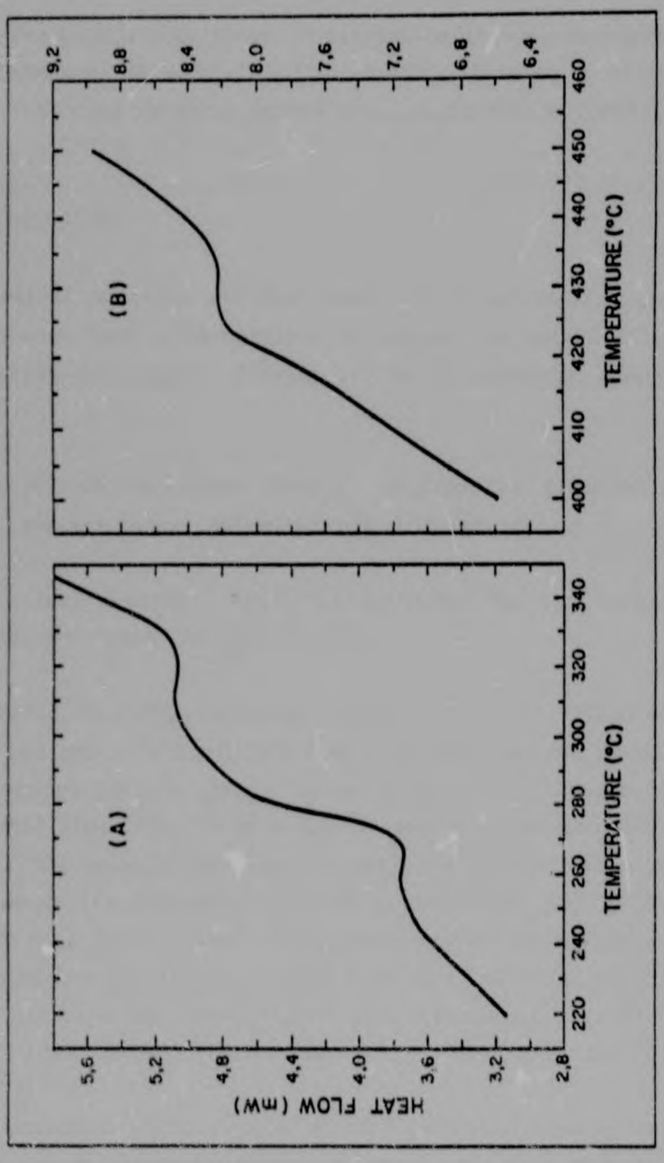

FIG 5.4

DSC profile of the transformation $Li_{\sim 0.45}VO_2 \rightarrow Li_{\sim 0.9}V_2O_4$

The spinel $Li_{\sim 0.9}V_2O_4$, which is lithium-deficient, is metastable, and decomposes at ~420 °C (fig. 5.4b), yielding a mixture of LiV_2O_5 and other vanadium oxides which could not be identified.

5.6 CONCLUSIONS

The chemical analyses and the powder X-ray diffraction patterns clearly show that it is possible to prepare the spinel $Li_{1-y}V_2O_4$ by heating $Li_{1-y/2}VO_2$ ($0<y<0.10$) to a moderate temperature (300 °C).

Similar routes have been used to prepare the titanium spinel $LiTi_2O_4$ and the nickel spinel $LiNi_2O_4$ [77,145,162].

In one case, anatase (TiO_2) was lithiated to the composition $Li_{0.5}TiO_2$ and heated to 700 °C [77].

In a thesis on A_xMO_2 compounds (where A = alkali cation and M = transition metal cation), M Maazaz also reported the preparation of the spinel $LiTi_2O_4$ [162]. In this case, $NaTiO_2$ which is isostructural with $LiMO_2$ (M = V, Co, Cr and Ni), was used as a precursor. The layered compound was refluxed in a solution of LiCl in methanol. The methanol was found to oxidise $NaTiO_2$ to the composition $Na_{\sim 0.5}TiO_2$; the latter underwent the ion exchange reaction, yielding $Li_{\sim 0.5}TiO_2$. Heat-treatment of this material at 100 °C led to a disordered defect rocksalt structure, which converted to the spinel $LiTi_2O_4$ upon further heating at 400 °C.

After completion of this work, a report was published on the preparation of the hitherto unknown spinel $Li[Ni_2]O_4$ [145]. The layered compound $LiNiO_2$, which is isostructural with $LiMO_2$ (M = V, Co, Cr), was delithiated electrochemically to the composition $Li_{\sim 0.5}NiO_2$; the structure of this compound could not be determined (cf section 4.6). This product forms the normal spinel $Li[Ni_2]O_4$ when heated to 200 °C [145].

It can thus be remarked that the compounds $Li_{\sim 0.5}MO_2$ (M = V, Ni, Ti) derived from the isostructural layered oxides $LiVO_2$, $LiNiO_2$ and, indirectly, $NaTiO_2$, convert to the spinel at relatively low temperatures (viz. 200-400 °C). This transformation only involves the migration of a fraction of the cations within the cubic-close-packed oxide lattice; it therefore requires relatively little energy.

A much higher temperature (viz. ~700 °C) is necessary to complete the transformation of lithiated anatase, $Li_{0.5}TiO_2$, to the spinel. In this case, the structure undergoes a more extensive transformation, requiring more energy: a rearrangement of the highly distorted cubic-close-packed oxide lattice of anatase accompanies the migration of Li^+ and $Ti^{3+/4+}$ cations through the layers.

Finally, the relative ease with which the spinels $Li_{\sim 1.0}[M_2]O_4$ (M = V, Ti, Ni) can be formed evidences the stability of the spinel structure, even in the case of slight cation-deficiency, and particularly if compared to a disordered defect rocksalt structure.

CHAPTER 6

LITHIUM INSERTION INTO LiV_2O_4

6.1 INTRODUCTION

As it was stated in section 1.4.3, the isomorphous spinels $LiTi_2O_4$, LiV_2O_4 and $LiMn_2O_4$ constitute a particularly interesting group of compounds as potential electrodes for secondary lithium cells.

Both lithium insertion into and extraction from the isostructural spinel $LiMn_2O_4$ have been thoroughly studied [33,74-76,100,163]. Lithiation of $LiTi_2O_4$ has been reported by Murphy et al. [77,78, 164].

The topochemical reactions of lithium with the spinel LiV_2O_4 have not yet been investigated. Lithium insertion into LiV_2O_4 is described in this chapter; delithiation of LiV_2O_4 will be reported in chapter 7. The structural and electrochemical characteristics of LiV_2O_4 will be compared with those of $LiTi_2O_4$ and $LiMn_2O_4$.

6.2 EXPERIMENTAL

The starting material $Li_{0.94}V_2O_4$ was prepared according to the route outlined in Chapter 5. The cell constant of this phase (a = 8.246 (1) Å) was characteristic of a lithium-deficient spinel, described by the expression $Li_{0.94}V_{0.06}[V_{1.94}\square_{0.06}]O_4$ (cf chapter 5). The precursor, $LiVO_2$, has recently been found to oxidise slowly when exposed to air [165]. In view of this, $LiVO_2$ was stored under argon, and assumed to have the composition $Li_{\sim 0.98}VO_2$. Samples of LiV_2O_4 subsequently prepared (and used for some of the electrochemical measurements) had a lithium content very close to that of $Li_yV_2O_4$ (where y = 1.00).

Lithium insertion was obtained by both chemical and electrochemical techniques.

Chemical lithiation was undertaken according to the method described in section 3.1. Various amounts of n-BuLi were added to 250 mg $Li_{\sim 1.0}V_2O_4$ in ~40 ml sodium-dried hexane. Reactions took place at 50 °C, with constant stirring, over a period of 2-3 days yielding samples with a lithium content of $0<x<0.86$ in $Li_{1+x}V_2O_4$ and 8 days for samples with the composition $Li_2V_2O_4$.

Lithium was inserted electrochemically into $Li_{0.94}V_2O_4$ at ambient temperature, in a two-electrode cell of the form:

$$Li/1M\ LiClO_4 \text{ in propylene carbonate } /Li_{0.94}V_2O_4$$

Cells were discharged at a constant current of 20 $\mu A/cm^2$. Open-circuit voltages were obtained intermittently after allowing equilibration times of up to 72 hours.

Galvanostatic (20 $\mu A/cm^2$) discharge curves were obtained with a similar cell, using 10 mg of $Li_{0.98}V_2O_4$, compacted onto a stainless-steel gauze disc at a pressure of 60 kN (18 MPa).

Cyclic voltammetry experiments were conducted according to the procedure described in section 3.3.2 and lithium diffusion rates were determined as described in section 3.3.3.

6.3 RESULTS

Lithiation of $Li_{\sim 1.0}V_2O_4$ proceeds smoothly up to the composition $Li_2V_2O_4$, beyond which no further lithium insertion was possible.

Powder X-ray diffraction profiles of the lithiated samples $Li_{1+x}V_2O_4$ ($0<x\leq 1$) showed retention of the spinel pattern, and could be indexed to the cubic space-group Fd3m.

The variation of the cell constant as a function of the composition $Li_{1+x}V_2O_4$ is shown in Fig. 6.1 and listed in Table 6.1.

TABLE 6.1: Cell constants of various $Li_{1+x}V_2O_4$ phases

Composition	a [Å]
$Li_{0.94}V_2O_4$	8.246 (1)
$Li_{1.27}V_2O_4$	8.246 (1)
$Li_{1.35}V_2O_4$	8.249 (2)
$Li_{1.47}V_2O_4$	8.250 (2)
$Li_{1.51}V_2O_4$	8.250 (1)
$Li_{1.80}V_2O_4$	8.278 (2)
$Li_{1.86}V_2O_4$	8.286 (4)
$Li_{2.0}V_2O_4$	8.291 (1)

During the initial stage of the reaction ($0<x<0.3$ in $Li_{1+x}V_2O_4$), the cell constant remains unaltered. As lithiation progresses ($0.3<x<0.5$), the lattice parameter rises more rapidly, to reach the final value a = 8.291 (1)Å in $Li_2V_2O_4$, which amounts to an expansion of the unit cell volume of 1.6%.

6.4 STRUCTURAL CHARACTERISATION OF $Li_{1.5}V_2O_4$ and $Li_2V_2O_4$

The intensity distribution in the powder X-ray diffraction patterns of the samples $Li_{1+x}V_2O_4$ ($0<x<0.5$) was very similar to LiV_2O_4. A change in the relative intensities is observed in samples with a higher lithium content ($x > 0.5$ in $Li_{1+x}V_2O_4$).

For this reason, two samples with the respective compositions $Li_{1.5}V_2O_4$ and $Li_2V_2O_4$ were selected for structure analysis. The structures were determined by intensity refinements of the powder X-ray diffraction patterns shown in Figs 6.2 and 6.3 and listed in Tables 6.2 and 6.3. Due to overlapping peaks, the refinements were carried out with 16 and 17 intensities, derived from 24 reflections, in the case of $Li_2V_2O_4$ and $Li_{1.5}V_2O_4$ respectively.

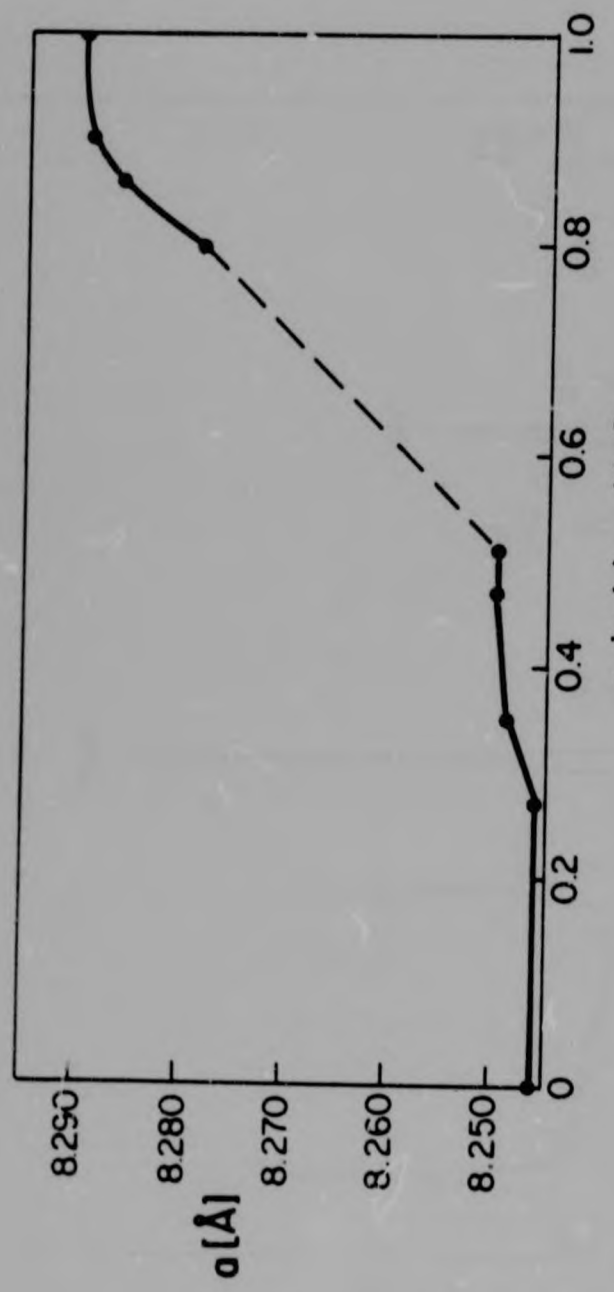

FIG. 6.1
Variation of the cell constant ("a") as a function of the composition $Li_{1+x}V_2O_4$

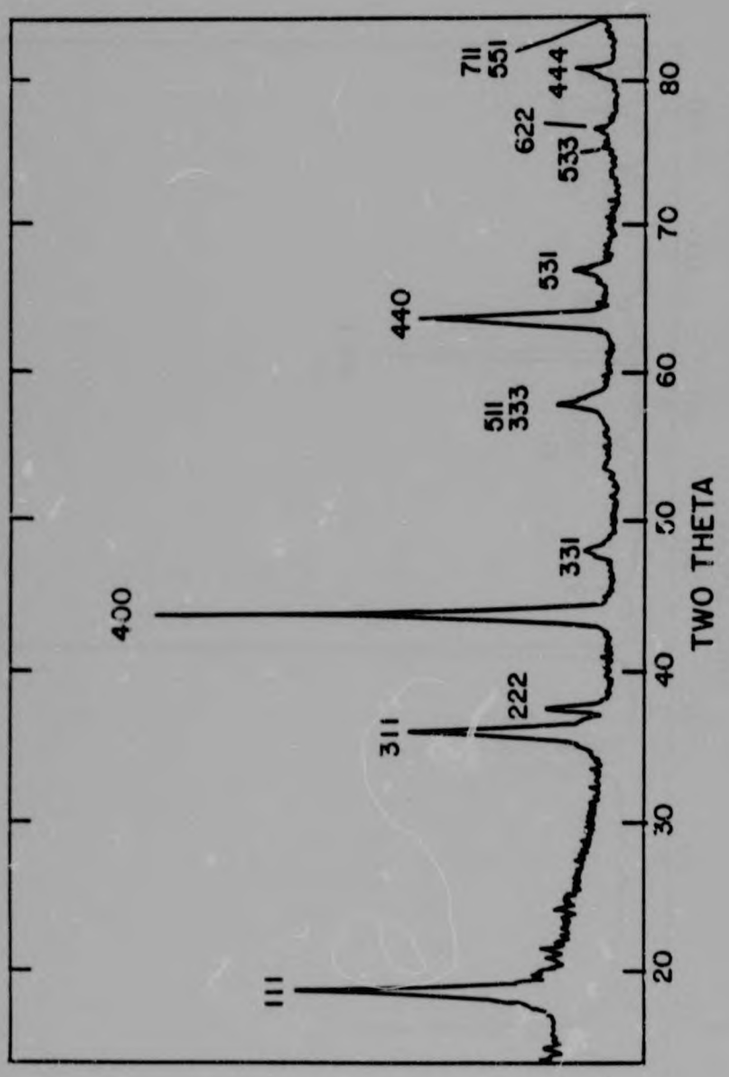

FIG. 6.2
X-ray diffraction pattern of $Li_{1.5}V_2O_4$

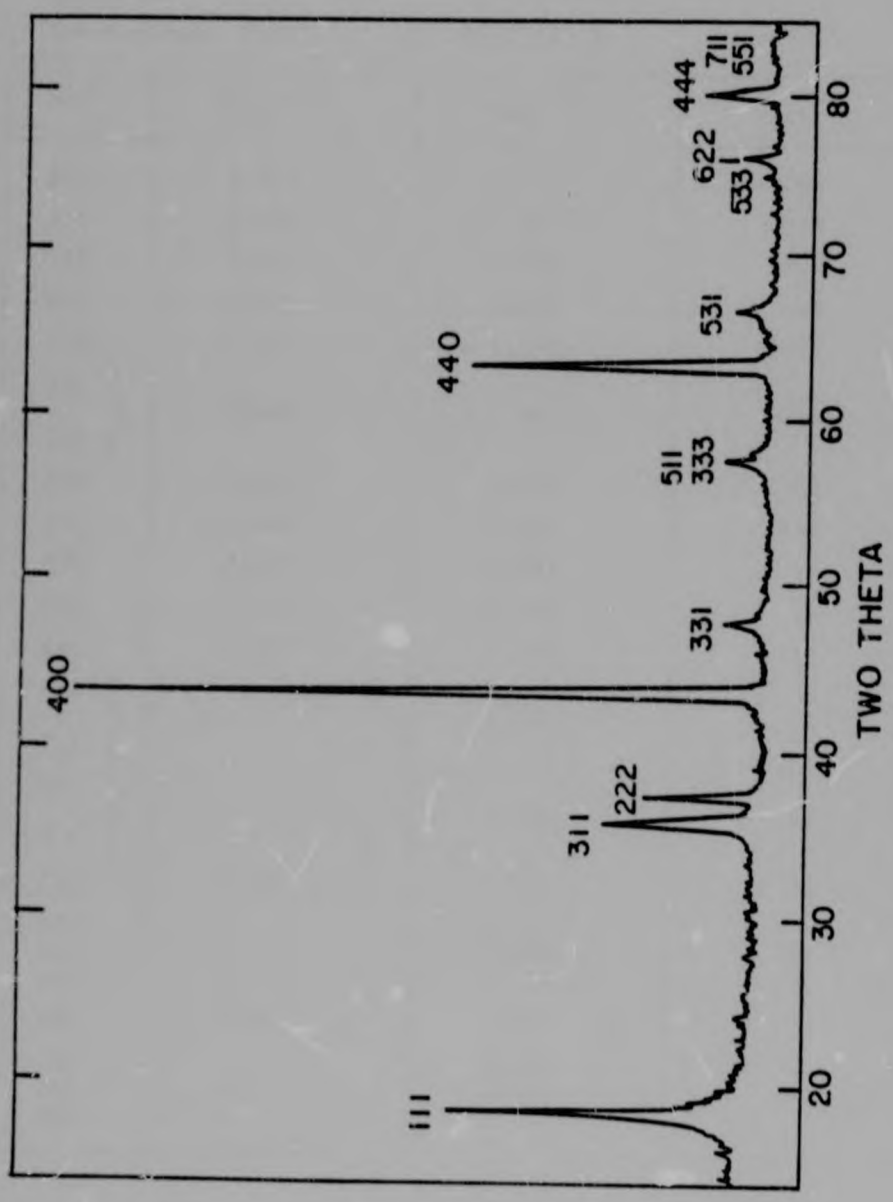

FIG. 6.3
X-ray diffraction pattern of $Li_{2.0}V_2O_4$

TABLE 6.2

Powder X-ray diffraction pattern of $Li_{1.5}V_2O_4$

Space group: Fd3m a = 8.250(1) Å α = 90 °

hkl	d_{obs}* [Å]	d_{calc} [Å]	I_{obs}**
111	4.777	4.763	1 000
311	2.486	2.487	588
222	2.380	2.382	109
400	2.062	2.062	868
331	1.893	1.893	79
511 333	1.588	1.588	215
440	1.458	1.458	500
531	1.394	1.394	156
533	1.259	1.258	56
622	1.243	1.244	76
444	1.190	1.191	117
551 711	-	1.159	71
553 731	-	1.074	69
800	1.030	1.031	76
751	-	0.953	
555	-	0.953	100
662	-	0.934	
840	0.921	0.922	174
753	-	0.906	
911	-	0.906	78
842	-	0.900	

* No d_{obs} is indicated for weak and diffuse peaks

** I_{obs} normalised to 1 000

TABLE 6.3

Powder X-ray diffraction pattern of $Li_{2.0}V_2O_4$

Space group: Fd3m a = 8.291(1) Å α = 90 °

hkl	d_{obs}* [Å]	d_{calc} [Å]	I_{obs}**
111	4.802	4.787	847
311	2.501	2.500	409
222	2.395	2.394	130
400	2.073	2.073	1 000
331	1.903	1.902	96
511	1.597	1.596	135
333			
440	1.466	1.466	472
531	1.401	1.401	124
533	-	1.264	114
622	1.250	1.250	
444	1.197	1.197	124
551	-	1.161	78
711			
553	-	1.079	55
731			
800	1.037	1.036	57
751	-	0.957	76
555	-	0.957	
662	-	0.951	
840	0.927	0.927	183
753	-	0.910	32
911		0.910	
842		0.905	

* No d_{obs} is indicated for weak and diffuse peaks

** I_{obs} normalised to 1 000

6.4.1 Structure determination of $Li_{1.5}V_2O_4$

In a preliminary refinement (Model 1), lithium was allowed to reside in both the tetrahedral 8a and the octahedral 16c sites. The total occupancy of lithium in those sites was restricted to 1.5. Although simultaneous occupation of the face-sharing 8a and 16c sites may seem unlikely, it has been shown to occur in $Li_2Mn_2O_4$, using neutron diffraction data [163].

The positional parameters and the isotropic temperature factors (B_{iso}) of the oxide ion were refined. The vanadium occupancy of the 16d sites was kept constant at 2.0; the B_{iso} factors of lithium and vanadium were fixed at 1.0 $Å^2$ and 0.1 $Å^2$ respectively.

The occupancy of lithium in the 8a and 16c sites refined to 0.9(3) and 0.6(3) respectively, indicating that, within experimental error, the lithium ions initially present in $Li[V_2]O_4$ remain in the 8a sites of the lithiated compound $Li_{1.5}V_2O_4$. The anion positional parameter and B_{iso} factor obtained were 0.259(2) and 1.8(7) $Å^2$ respectively.

This model yielded a reliability factor of 8.6%. The full structural parameters of $Li_{1.5}V_2O_4$ according to model 1 are given in Table 6.4a, the observed and calculated intensities in Table 6.4b.

The cell constant of the starting material (a = 8.246(1) Å) was characteristic of a slightly lithium-deficient vanadium spinel. It is therefore suggested that, in the lithiated compound, a fraction of the vanadium cations is situated either in the 8a sites (Model 2), as in $(Li_{1-y}V_y)_{8a}[V_{2-y}\square_y]O_4$ $(0<y\leq0.1)$ (cf chapter 5), or in the 16c positions (Model 3), since transition metal cations are known to be co-operatively displaced from the 8a to the 16c sites during an early stage of the lithiation of spinels [28,33,81].

6.4.1 Structure determination of $Li_{1.5}V_2O_4$

In a preliminary refinement (Model 1), lithium was allowed to reside in both the tetrahedral 8a and the octahedral 16c sites. The total occupancy of lithium in those sites was restricted to 1.5. Although simultaneous occupation of the face-sharing 8a and 16c sites may seem unlikely, it has been shown to occur in $Li_2Mn_2O_4$, using neutron diffraction data [163].

The positional parameters and the isotropic temperature factors (B_{iso}) of the oxide ion were refined. The vanadium occupancy of the 16d sites was kept constant at 2.0; the B_{iso} factors of lithium and vanadium were fixed at 1.0 $Å^2$ and 0.1 $Å^2$ respectively.

The occupancy of lithium in the 8a and 16c sites refined to 0.9(3) and 0.6(3) respectively, indicating that, within experimental error, the lithium ions initially present in $Li[V_2]O_4$ remain in the 8a sites of the lithiated compound $Li_{1.5}V_2O_4$. The anion positional parameter and B_{iso} factor obtained were 0.259(2) and 1.8(7) $Å^2$ respectively.

This model yielded a reliability factor of 8.6%. The full structural parameters of $Li_{1.5}V_2O_4$ according to model 1 are given in Table 6.4a, the observed and calculated intensities in Table 6.4b.

The cell constant of the starting material (a = 8.246(1) Å) was characteristic of a slightly lithium-deficient vanadium spinel. It is therefore suggested that, in the lithiated compound, a fraction of the vanadium cations is situated either in the 8a sites (Model 2), as in $(Li_{1-y}V_y)_{8a}[V_{2-y}\square_y]O_4$ $(0<y<0.1)$ (cf chapter 5), or in the 16c positions (Model 3), since transition metal cations are known to be co-operatively displaced from the 8a to the 16c sites during an early stage of the lithiation of spinels [28,33,81].

TABLE 6.4a

Structural parameters of $Li_{1.5}V_2O_4$ (Model 1)

R = 8.6%

Space group: $Fd3m$ (O_h^7) a = 8.250(1) Å

Atom	Position	x	y	z	B[Å^2]	n
Li^+	8a	0.125	0.125	0.125	1.0	0.9(3)
Li^+	16c	0.000	0.000	0.000	1.0	0.6(3)
$V^{3+/4+}$(*)	16d	0.500	0.500	0.500	0.1	2.0
O^{2-}	32e	0.259(2)	0.259(2)	0.259(2)	1.8(7)	4.0

* Mean oxidation state of vanadium: 3.25

TABLE 6.4b

Observed and calculated intensities for $Li_{1.5}V_2O_4$ (Model 1)

hkl	I obs	I calc	hkl	I obs	I calc
111	1 072	1 147	551 }	76	81
311	630	571	711 }		
222	117	47	553 }	74	90
400	931	928	731 }		
331	85	124	800	81	61
511 }	230	235	751 }	107	122
333 }			555 }		
			662 }		
440	536	495	840	187	181
531	170	158	753 }	84	74
533	60	56	911 }		
			842 }		
622	81	65			
444	125	120			

TABLE 6.4a

Structural parameters of $Li_{1.5}V_2O_4$ (Model 1)

R = 8.6%

Space group: $Fd3m$ (O_h^7) a = 8.250(1) Å

Atom	Position	x	y	z	B[Å^2]	n
Li^+	8a	0.125	0.125	0.125	1.0	0.9(3)
Li^+	16c	0.000	0.000	0.000	1.0	0.6(3)
$V^{3+/4+}$(*)	16d	0.500	0.500	0.500	0.1	2.0
O^{2-}	32e	0.259(2)	0.259(2)	0.259(2)	1.8(7)	4.0

* Mean oxidation state of vanadium: 3.25

TABLE 6.4b

Observed and calculated intensities for $Li_{1.5}V_2O_4$ (Model 1)

hkl	I obs	I calc	hkl	I obs	I calc
111	1 072	1 147	551, 711	76	81
311	530	571			
222	117	47	553, 731	74	90
400	931	928			
331	85	124	800	81	61
511, 333	230	235	751, 555, 662	107	122
440	536	495	840	187	181
531	170	158	753, 911, 842	84	74
533	60	56			
622	81	65			
444	123	120			

In Model 2, the lithium cations occupy the 8a and 16c sites, whilst the vanadium cations occupy the 8a and 16d sites. The total lithium and vanadium contents were restricted to 1.5 and 2.0 respectively. Isotropic temperature factors of lithium and vanadium were fixed at 1.0 $Å^2$ and 0.1 $Å^2$ respectively, as in Model 1. The oxide ion positional parameter was maintained at the value found in the course of the first refinement, i.e. 0.259, and the B_{iso} factor was fixed at 2.0 $Å^2$.

Lithium occupancies refined to 0.4(3) and 1.1(3) in the 8a and 16c sites respectively; the final vanadium occupancies were 0.07(4) in the 8a and 1.93(4) in the 16d positions. The final structural parameters for Model 2 are listed in Table 6.5a, the observed and calculated intensities in Table 6.5b.

Although the R value (7.1%) indicates a significant improvement over Model 1, where all the vanadium cations reside in the 16d sites, this structure does not seem reasonable. According to this model, a migration from the tetrahedral (8a) to the octahedral (16c) sites of approximately 50% of the lithium ions occurs more readily than a similar transfer of a fraction of vanadium cations.

This is unlikely, since the interaction between the inserted lithium ions in the 16c sites and the pentavalent vanadium cations in the tetrahedral sites would be expected to displace the V^{5+} ions before the monovalent lithium cations, which occupy equivalent sites. Upon migration from the tetrahedral 8a to the octahedral 16c sites, the V^{5+} cations capture an electron and are reduced to V^{4+} ions.

In the final structure (Model 3), the vanadium cations occupy the 16c and 16d octahedral sites, whilst the lithium cations were distributed in the 8a and 16c sites. As in previous models, the total lithium and vanadium concentrations were constrained to 1.5 and 2.0, in accordance with the chemical formula. The B_{iso}

TABLE 6.5a

Structural parameters of $Li_{1.5}V_2O_4$ (Model 2)

R = 7.1%

Space group: $Fd3m$ (O_h^7) a = 8.250(1) Å

Atom	Position	x	y	z	B[Å^2]	n
Li^+	8a	0.125	0.125	0.125	1.0	0.4(3)
Li^+	16c	0.000	0.000	0.000	1.0	1.1(3)
V^{5+}	8a	0.125	0.125	0.125	0.1	0.07(4)
$V^{3+/4+}$*	16d	0.500	0.500	0.500	0.1	1.93(4)
O^{2-}	32e	0.259(2)	0.295(2)	0.259(2)	2.0	4.0

* Mean oxidation state of vanadium: 3.25

TABLE 6.5b

Observed and calculated intensities for $Li_{1.5}V_2O_4$ (Model 2)

hkl	I obs	I calc	hkl	I obs	I calc
111	1 072	1 078	551	76	75
311	630	574	711		
222	117	50	553	74	92
400	931	978	731		
331	85	109	800	81	65
511	230	238	751	107	130
333			555		
			662		
440	536	534	840	187	182
531	170	146	753	84	68
533	60	56	911		
			842		
622	81	72			
444	125	123			

factor for Li^+ was fixed arbitrarily at 1.0 $Å^2$ and at 0.1 $Å^2$ for the vanadium cations, as lithium is anticipated to be highly mobile in the 8a - 16d channels, whereas the vanadium cations are expected to undergo little motion. The oxide positional coordinates and isotropic temperature factor were fixed at the values obtained during previous refinements. In the final cycle, the vanadium B_{iso} factor was refined and the value of 0.1(2) was obtained, in agreement with the figure arbitrarily assigned during the refinement.

According to this model, lithium occupancies in the 8a and 16c sites refined to 1.2(3) and 0.3(3) respectively, whilst the vanadium occupancies were 1.92(4) in the 16d and 0.08(4) in the 16c sites. The final R value for this model was 6.7%. The full atomic parameters for Model 3 are given in Table 6.6a, the observed and calculated intensities in Table 6.6b. Taking into account the weak scattering power of the Li^+ cations, and the error in the lithium occupancy, Model 3 would appear to offer the most reasonable structure; a likely cation distribution in $Li_{1.5}V_2O_4$ is therefore described by the expression $(Li_{1.0})_{8a}\{Li_{0.5}V_{0.06}\}_{16c}[V_{1.94}\square_{0.06}]_{16d}O_4$.

6.4.2 Structure determination of $Li_{2.0}V_2O_4$

Although the diffraction patterns of $Li_{1.5}V_2O_4$ and $Li_{2.0}V_2O_4$ are very similar, significant changes in the relative intensities of a few reflections are observed. In particular, the ratio $I\{222\}/I\{311\}$ increases from 0.15 in LiV_2O_4 (0.13 in $Li_{0.9}V_2O_4$) to 0.32 in $Li_2V_2O_4$. This change indicates increased cation occupancy of the 16c and 16d octahedral sites and decreased scattering by cations in the 8a sites (cf Appendix).

A preliminary refinement of the structure indicated that all the lithium cations were situated in the octahedral 16c sites. During the first cycle of the refinement, the Li^+ ions were placed in

TABLE 6.6a

Structural parameters of $Li_{1.5}V_2O_4$ (Model 3)

R = 6.7%

Space group: $Fd3m$ (O_h^7) a = 8.250(1) Å

Atom	Position	x	y	z	B[Å^2]	n
Li^+	8a	0.125	0.125	0.125	1.0	1.2(3)
Li^+	16c	0.000	0.000	0.000	1.0	0.3(3)
$V^{3+/4+}$*	16c	0.000	0.000	0.000	0.1	0.08(4)
$V^{3+/4+}$*	16d	0.500	0.500	0.500	0.1(2)	1.92(4)
O^{2-}	32e	0.259(2)	0.259(2)	0.259(2)	2.0	4.0

* Mean oxidation state of vanadium: 3.2

TABLE 6.6b

Observed and calculated intensities for $Li_{1.5}V_2O_4$ (Model 3)

hkl	I_{obs}	I_{calc}	hkl	I_{obs}	I_{calc}
111	1 072	1 075	551 }	76	74
311	630	578	711 }		
222	117	50	553 }	74	90
400	931	978	731 }		
331	85	108	800	81	65
511 }	230	239	751 }	107	129
333 }			555 }		
			662 }		
440	536	536	840	187	187
531	170	145	753 }	84	68
533	60	56	911 }		
622	81	72	842 }		
444	125	124			